© 2020. Published by The Company of Biologists Ltd | Development (2020) 147, dev185850. doi:10.1242/dev.185850

RESEARCH ARTICLE

A developmental gene regulatory network for *C. elegans* anchor cell invasion

Taylor N. Medwig-Kinney[1,*], Jayson J. Smith[1,*], Nicholas J. Palmisano[1], Sujata Tank[1,2], Wan Zhang[1] and David Q. Matus[1,‡]

ABSTRACT

Cellular invasion is a key part of development, immunity and disease. Using an *in vivo* model of *Caenorhabditis elegans* anchor cell invasion, we characterize the gene regulatory network that promotes cell invasion. The anchor cell is initially specified in a stochastic cell fate decision mediated by Notch signaling. Previous research has identified four conserved transcription factors, *fos-1* (Fos), *egl-43* (EVI1/MEL), *hlh-2* (E/Daughterless) and *nhr-67* (NR2E1/TLX), that mediate anchor cell specification and/or invasive behavior. Connections between these transcription factors and the underlying cell biology that they regulate are poorly understood. Here, using genome editing and RNA interference, we examine transcription factor interactions before and after anchor cell specification. Initially, these transcription factors function independently of one another to regulate LIN-12 (Notch) activity. Following anchor cell specification, *egl-43*, *hlh-2* and *nhr-67* function largely parallel to *fos-1* in a type I coherent feed-forward loop with positive feedback to promote invasion. Together, these results demonstrate that the same transcription factors can function in cell fate specification and differentiated cell behavior, and that a gene regulatory network can be rapidly assembled to reinforce a post-mitotic, pro-invasive state.

KEY WORDS: EGL-43, FOS-1, HLH-2, NHR-67, Gene regulatory network, Cell invasion, Cell cycle arrest

INTRODUCTION

Invasion through basement membranes (BMs) is a cellular behavior that is integral to embryo placentation, tissue patterning during embryonic development, and immune response to infection and injury (Medwig and Matus, 2017; Rowe and Weiss, 2008). Increased cellular invasiveness is also a hallmark of metastatic cancer (Hanahan and Weinberg, 2011). Previous research has identified several cell-autonomous mechanisms that are highly conserved across different contexts of BM invasion (Kelley et al., 2014; Medwig and Matus, 2017). These include localization of F-actin and upregulation of matrix metalloproteinases (MMPs) to chemically degrade the BM (Hagedorn et al., 2009, 2013; Kelley et al., 2019; Levitan and Greenwald, 1998; Morrissey et al., 2014; Sherwood et al., 2005). There is also growing evidence that cells must undergo cell cycle arrest in order to invade the BM (Kohrman and Matus, 2017; Matus et al., 2015). How these tightly coordinated programs are transcriptionally regulated is not well understood.

[1]Department of Biochemistry and Cell Biology, Stony Brook University, Stony Brook, NY 11794-5215, USA. [2]Science and Technology Research Program, Smithtown High School East, St. James, NY 11780-1833, USA.
*These authors contributed equally to this work

‡Author for correspondence (david.matus@stonybrook.edu)

T.N.M.-K., 0000-0001-7989-3291; N.J.P., 0000-0002-7992-4462; D.Q.M., 0000-0002-1570-5025

Received 2 July 2019; Accepted 25 November 2019

As many contexts of cellular invasion occur deep within tissue layers and are thus difficult to visualize, we utilize morphogenesis of the *Caenorhabditis elegans* uterine-vulval connection as a genetically tractable and visually amenable model for examining cell invasion *in vivo* (Sherwood and Sternberg, 2003). During the mid-L3 stage, a specialized uterine cell called the anchor cell (AC), invades the underlying BM, connecting the uterus to the vulval epithelium to facilitate egg laying (Fig. 1A,B) (Sherwood and Sternberg, 2003). The AC itself is specified in a cell fate decision event earlier in development, during the L2 stage, when two initially equipotent cells diverge via stochastic Notch asymmetry, giving rise to the terminally differentiated AC and a proliferative ventral uterine (VU) cell (Fig. 1A,B) (Wilkinson et al., 1994).

Prior research has identified four pro-invasive transcription factors (TFs) that function cell-autonomously to regulate AC invasion (Fig. 1A). These include the basic leucine zipper TF *fos-1* (Fos), the basic helix-loop-helix TF *hlh-2* (E/Daughterless), the nuclear hormone receptor *nhr-67* (NR2E1/Tailless/TLX) and the zinc-finger TF *egl-43* (EVI1/MEL) (Hwang et al., 2007; Matus et al., 2010; Rimann and Hajnal, 2007; Schindler and Sherwood, 2011; Sherwood et al., 2005; Verghese et al., 2011). NHR-67 functions upstream of the cyclin-dependent kinase inhibitor CKI-1 (p21/p27), to induce G1/G0 cell cycle arrest, which is necessary for AC invasion (Matus et al., 2015). Independently of NHR-67 activity, FOS-1A regulates the expression of the long isoform of *egl-43* (EGL-43L) and downstream effectors including multiple MMPs (*zmp-1*, *-3* and *-6*) and a cadherin (*cdh-3*) (Hwang et al., 2007; Kelley et al., 2019; Matus et al., 2010; Rimann and Hajnal, 2007). HLH-2 independently regulates *cdh-3* along with other targets and cytoskeletal polarity (Schindler and Sherwood, 2011). Prior work has also suggested that EGL-43 and HLH-2 may regulate NHR-67 based on conserved HLH-2 binding motifs present in the *nhr-67* promoter as well as perturbation experiments using *nhr-67* transgenic reporters (Bodofsky et al., 2018; Verghese et al., 2011). Interestingly, three of these TFs (*egl-43*, *hlh-2* and *nhr-67*) also play key roles in the specification of the AC and VU cell fates during the L2 stage (Attner et al., 2019; Hwang et al., 2007; Karp and Greenwald, 2004; Sallee et al., 2017; Verghese et al., 2011). How these four TFs function, independently and together, to regulate both specification and invasive activity of the differentiated AC is poorly understood.

Here, using new highly efficient RNA interference (RNAi) vectors (Sturm et al., 2018), we identify novel roles for *egl-43* and *hlh-2* in maintaining the AC in a cell cycle-arrested state. Additionally, we generated GFP knock-in alleles for each pro-invasive TF using CRISPR/Cas9-mediated genome engineering. These tools allow for quantitative measures of endogenous protein in the context of native chromatin architecture and potential distal enhancer elements that may be misrepresented using traditional transgenic reporters (Dickinson and Goldstein, 2016; Dickinson et al., 2013; Kim et al., 2014). Using these alleles and improved RNAi constructs, we report

Development (2020) 147, dev185850. doi:10.1242/dev.185850

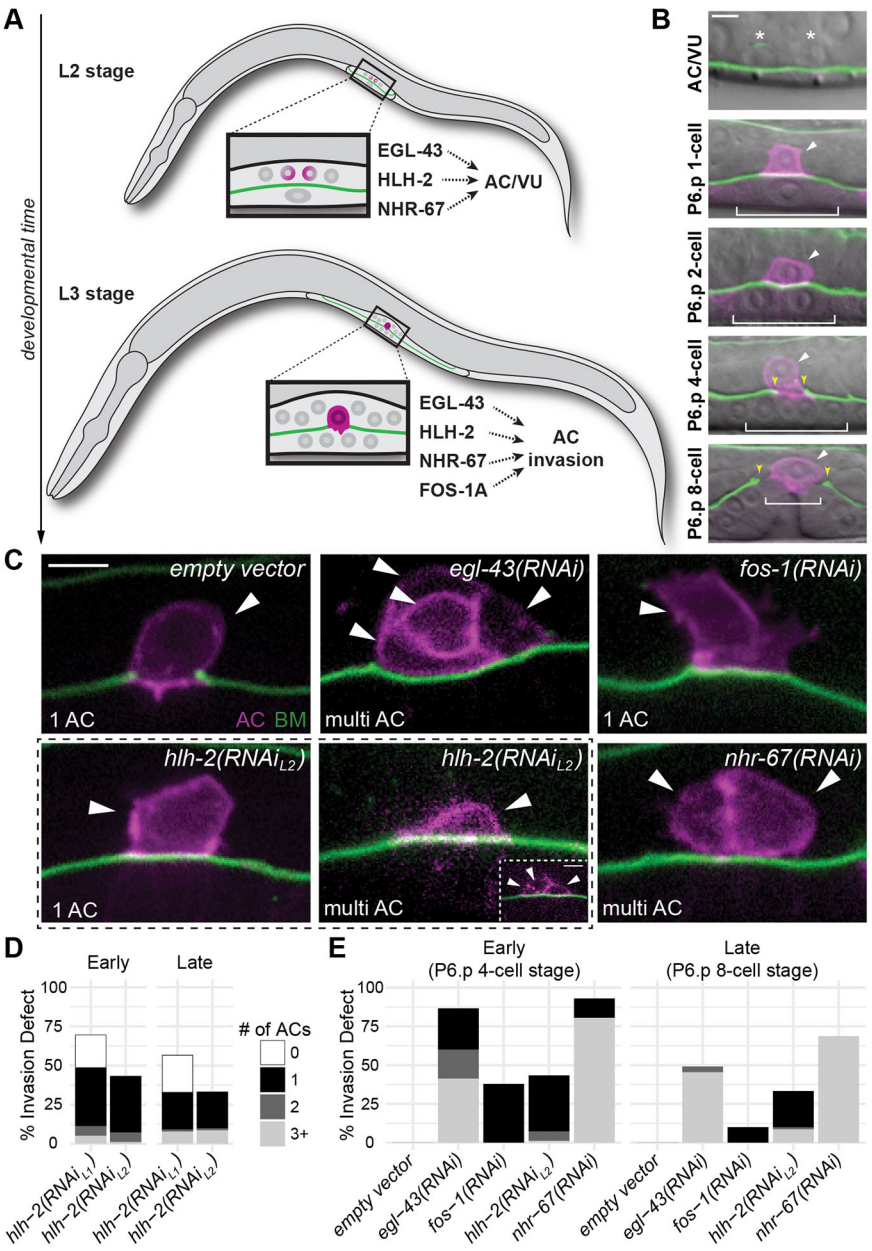

Fig. 1. RNAi depletion of pro-invasive TFs leads to defects in invasion and proliferation. (A) Schematic depicting the reiterative use of TFs in AC specification and invasion. (B) Micrographs depicting AC (magenta, *cdh-3*$^{1.5}$>mCherry::PLCδ^{PH}) specification and BM (green, *lam-1*>LAM-1::GFP) invasion over developmental time. Brackets indicate 1° VPCs. Yellow and white arrowheads indicate the BM breach and ACs, respectively. Asterisks indicate the AC/VU precursors, Z1.ppp and Z4.aaa. (C) Representative empty vector control and TF-RNAi depletion phenotypes, with multiple ACs from additional confocal *z*-planes shown as insets. Arrowheads indicate ACs. (D,E) Stacked bar charts showing the penetrance of invasion defects, binned by number of ACs, following TF-RNAi depletion (P<0.00001, Fisher's exact test, empty vector compared with each TF RNAi, n≥50 animals examined for each treatment). Because of the penetrance of the zero AC phenotype in early *hlh-2(RNAi)*-treated animals (D), an L2-plating strategy was used to assess post-specification AC invasion phenotypes (E). Scale bars: 5 µm.

the onset of relative expression of pro-invasive TFs in the lineages leading to the AC and dissect their molecular epistatic interactions. We find that, prior to AC/VU specification, *egl-43*, *hlh-2* and *nhr-67* function independently to regulate an endogenously tagged *lin-12*::GFP allele. This network appears to be assembled following specification, with the addition of a fourth node, *fos-1*, and activation of TF interactions. Furthermore, we characterized both a cell cycle-independent circuit and a cell cycle-dependent feed-forward regulatory circuit with positive feedback that is crucial for maintaining the AC in an invasive, post-mitotic state. These findings provide new insights into how a set of reiteratively used TFs can be re-purposed from regulating cell fate specification to coordinating a differentiated cellular behavior.

RESULTS

EGL-43 or HLH-2 RNAi depletion results in extra ACs

Our initial goal was to determine interactions between the four pro-invasive TFs *fos-1*, *egl-43*, *hlh-2* and *nhr-67*. To accomplish this, we first generated new RNAi targeting constructs in the improved RNAi vector, T444T, which includes T7 termination sequences to prevent the generation of non-specific RNA fragments from the vector backbone, increasing the efficacy of gene silencing over the original RNAi targeting vector, L4440 (Fig. S1A) (Sturm et al., 2018). As three of four pro-invasive TFs (*egl-43*, *hlh-2* and *nhr-67*) also function during AC specification (Attner et al., 2019; Hwang et al., 2007; Karp and Greenwald, 2004; Sallee et al., 2017; Verghese et al., 2011), we assessed TF depletions in a genetic background in which only the AC and neighboring uterine cells are sensitive to RNAi following the AC/VU decision (Matus et al., 2010). The uterine-specific RNAi-sensitive strain was generated through tissue-specific restoration of the RDE-1 Piwi/Argonaut protein in an *rde-1* mutant background using the *fos-1* promoter, which is expressed specifically in the somatic gonad during the late L2/early L3 stage of larval development (Haerty et al., 2008; Hagedorn et al., 2009; Matus et al., 2010, 2015). AC invasion was quantified as the presence or absence of a BM gap, visualized by laminin::GFP, at the P6.p four-cell stage, a

Development (2020) 147, dev185850. doi:10.1242/dev.185850

developmental window in which 100% of wild-type ACs are invaded (Fig. 1C, Table S1). We also assessed invasion several hours later, following vulval morphogenesis, allowing us to distinguish between delays in invasion and complete loss of invasive capacity (Fig. 1E, Fig. S1D, Table S1). Depletion of each TF resulted in invasion defects ranging from moderate penetrance (38%; *fos-1*) to highly penetrant (69-94%; *hlh-2*, *egl-43* and *nhr-67*), when synchronized L1-stage animals were plated on RNAi bacteria and scored at the mid-L3 stage (P6.p four-cell stage) and early L4 stage (P6.p eight-cell stage) (Fig. 1C-E, Fig. S1D). Consistent with previous work, depletion of *fos-1* resulted in single ACs that failed to breach the BM. Depletion of *nhr-67* resulted in proliferative, non-invasive ACs at a high penetrance. Depletion of *egl-43* phenocopied *nhr-67*, with a highly penetrant defect of multiple, non-invasive ACs. Lastly, depletion of *hlh-2* resulted in pleiotropic phenotypes in the AC, from animals with zero, one, two or even, in several cases, three or more ACs (Fig. 1D, Fig. S1C). In all cases, the penetrance of AC invasion defects was significantly increased using a T444T-based RNAi targeting vector compared with L4440-based vectors (Fig. S1A). Thus, use of the improved RNAi vector revealed unreported phenotypes resulting from depletion of *egl-43* and *hlh-2* during invasion, phenocopying depletion of *nhr-67* resulting in multiple non-invasive ACs (Matus et al., 2015).

Because of the pleiotropy associated with *hlh-2* depletion, which affects AC specification and invasion (Schindler and Sherwood, 2011), we sought to rule out the possibility that the extra *cdh-3*-expressing ACs are due to defects in AC specification. Depletions using the traditional RNAi vector L4440 in the uterine-specific RNAi-sensitive background is sufficient to bypass AC fate specification defects that occur in genetic backgrounds in which all cells are sensitive to RNAi (Matus et al., 2010). Specifically, loss of HLH-2 prior to AC specification disrupts the *lin-12*(Notch)/*lag-2*(Delta)-dependent signaling cascade, resulting in both pre-AC/VU cells adopting a VU fate and thereby producing a zero AC phenotype. During AC specification, loss of HLH-2 results in upregulation of pro-AC fate by activating *lag-2*/Delta resulting in both AC/VU cells adopting an AC fate (Karp and Greenwald, 2004; Schindler and Sherwood, 2011). Notably, *hlh-2* depletion using the T444T vector resulted in a greater occurrence of a zero AC phenotype compared with the L4440 *hlh-2* RNAi clone (Fig. 1D, Fig. S1A). This is likely due to the improved efficiency of RNAi-mediated knockdown using the enhanced T444T vector (Martinez et al., 2019), as the time period between restoration of RDE-1 function and the timing of the AC/VU decision appears decreased. Thus, to bypass these potential specification defects due to increased RNAi penetrance for *hlh-2* using the T444T vector, we depleted *hlh-2* and the other TFs by RNAi using an L2-plating strategy (Schindler and Sherwood 2011), growing animals to the time of the L1/L2 molt on OP50 *Escherichia coli* and then transferring them to TF-RNAi plates. L2 platings resulted in a lower overall penetrance of AC invasion defects for all TF-RNAi treatments (Fig. S1B), including *hlh-2* (43% at the P6.p four-cell stage; Fig. 1D) but all animals possessed an AC. Strikingly, some animals possessed multiple *cdh-3*-expressing ACs at the P6.p four-cell stage (Fig. 1C), and 10% of animals in the early L4 stage possessed multiple ACs (Fig. 1C-E, Fig. S1C,D). As the number of ACs increased over developmental time (Fig. 1D,E), these results suggest that the multiple ACs observed could be arising through loss of G1/G0-cell cycle arrest and *nhr-67* activity (Matus et al., 2015).

Characterization of GFP-tagged alleles and RNAi penetrance

Next, we sought to examine the relationship of these four TFs in the AC prior to and during invasion by combining gene knockdown with endogenous GFP-tagged alleles. To accomplish this, we used CRISPR/Cas9 genome-editing technology to knock in a codon-optimized GFP tag into the endogenous locus of each TF (Fig. S2, Tables S4-S6) (Dickinson and Goldstein, 2016). First, we examined a minimum of 50 L1/L2-stage animals to determine the onset of expression for each TF in the somatic gonad, which is derived from two founder cells, Z1 and Z4 (Kimble and Hirsh, 1979). The two cells that can stochastically give rise to the AC are the proximal great-granddaughters of Z1 and Z4 (Z1.ppp and Z4.aaa). Examination of L1- and L2-stage somatic gonads revealed that *egl-43*::*GFP::egl-43* turns on first, in Z1 and Z4, and remains on in their descendants through the time of AC/VU specification (Fig. 2A). As reported recently (Attner et al., 2019), *GFP::hlh-2* turns on at the second division of Z1/Z4 cells in Z1.pp and Z4.aa. We also detected onset of *nhr-67::GFP* in these cells in some animals, though it appears that their expression is weaker in Z1.pp/Z4.aa compared with *GFP::hlh-2*, but becomes robust in the AC/VU cells prior to specification. Finally, we detected weak expression of *GFP::fos-1* in L1 and L2 Z1/Z4 descendants that increased rapidly in the somatic gonad following AC specification (Fig. 2A). In summary, consistent with previously reported roles for *egl-43*, *hlh-2* and *nhr-67* in AC/VU specification (Hwang et al., 2007; Karp and Greenwald, 2004; Verghese et al., 2011), we detected the presence of endogenous GFP-tagged TFs in Z1/Z4 descendants.

Next, we examined the expression patterns of *TF::GFP* alleles following AC specification. All four TFs showed robust GFP localization in the AC nucleus prior to and during invasion (Fig. 2B). Additionally, the GFP-tagged strains had similar expression domains in the somatic gonad during the L3 larval stage as previously reported by traditional multi-copy array transgenes (Hwang et al., 2007; Rimann and Hajnal, 2007; Sherwood et al., 2005; Verghese et al., 2011). After examining expression patterns, we then synchronized TF GFP-tagged strains and collected a developmental time course quantifying the expression of GFP-tagged protein in the AC during uterine/vulval development (Fig. 2B). All GFP-tagged TFs were imaged using uniform acquisition settings on a spinning disk confocal microscope using an EM-CCD camera, allowing us to compare relative expression levels of endogenous GFP-tagged proteins in the AC. Interestingly, all four TFs followed the same general trend in expression levels, with a gradual increase in levels prior to invasion, peaking at or just before the P6.p four-cell stage when 100% of wild-type animals have generated a gap in the BM. Expression levels then decreased following invasion, during vulval morphogenesis, in the early L4 stage (P6.p eight-cell stage) (Fig. 2C,D).

To visualize invasion, we first crossed a BM reporter (*laminin::GFP*) and an AC marker (*cdh-3>mCherry:moeABD*; see Materials and Methods for transgene nomenclature) into each endogenously GFP-tagged TF strain. We then performed a series of RNAi depletion experiments targeting each TF and examining synchronized animals at the P6.p 4-cell stage. As the insertion of GFP tags into native genomic loci can potentially interfere with gene function, we examined a minimum of 50 animals treated with control (T444T) empty vector RNAi (Fig. S3). All four GFP-tagged strains showed 100% BM breach at the normal time of invasion in control animals (empty vector) (Fig. S3) and the animals all appeared superficially wild type. Additionally, all alleles generated did not appear to affect viability or fertility. Although this does not rule out other more subtle hypomorphic phenotypes, for the purpose of determining TF regulatory relationships during AC invasion, we consider all alleles generated to be equivalent to wild-type AC invasion.

As RNAi penetrance can be difficult to measure at the single cell level across a population, we next assessed the efficacy of our newly

Development (2020) 147, dev185850. doi:10.1242/dev.185850

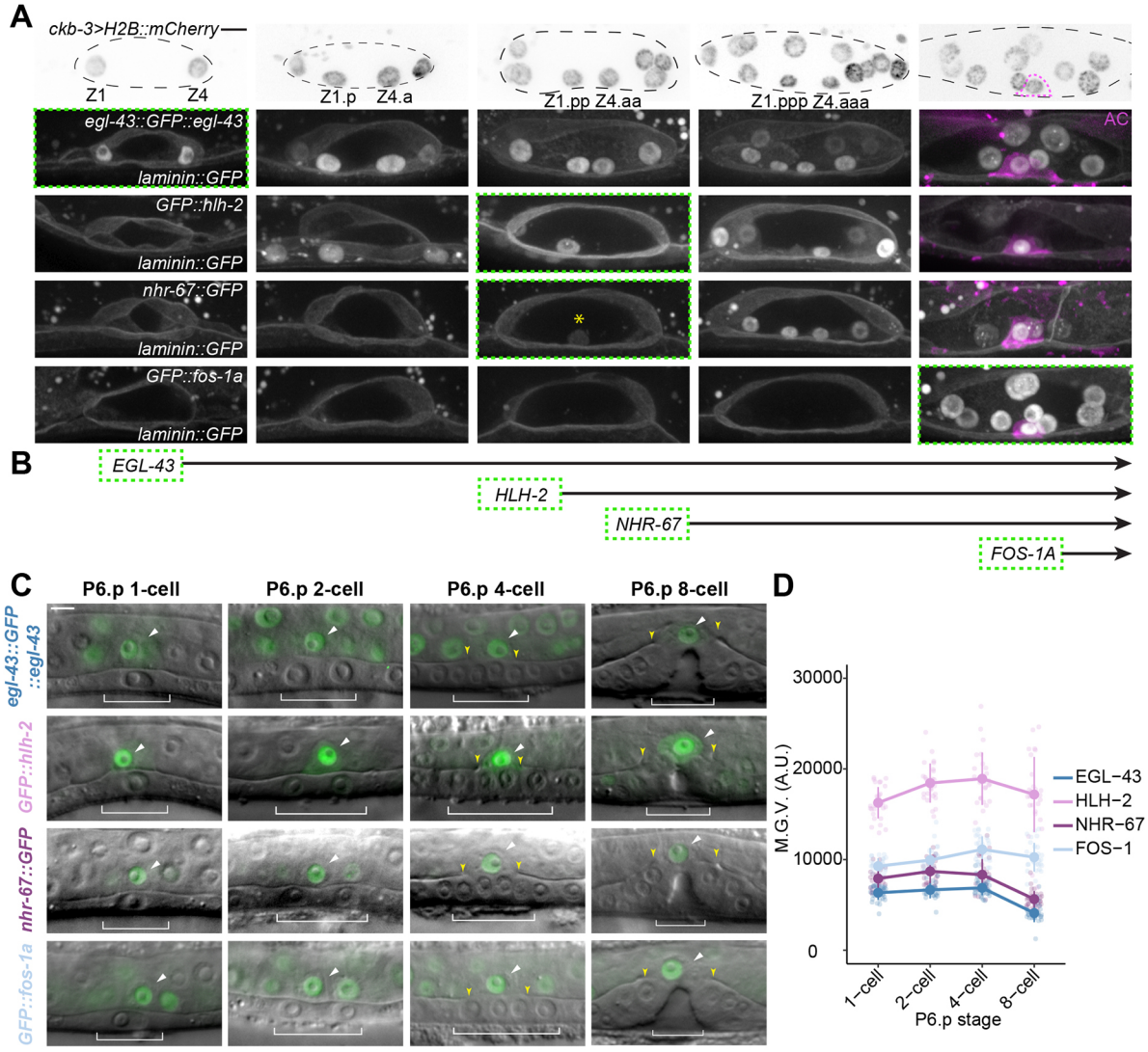

Fig. 2. Onset and expression of GFP-tagged alleles in the AC over developmental time. (A) Maximum intensity projections of GFP-tagged TFs (bottom) in the context of the BM-lined uterus (*laminin*::GFP), in relation to the number of somatic cells in the gonad (top; *ckb-3*>H2B::mCherry, inverted). Dashed green boxes indicate onset of TF expression. Dashed magenta line encircles the AC. Asterisk highlights weak TF expression. (B) Schematic illustrating the order of onset of pro-invasive TFs in Z1/Z4 descendants over time ($n \geq 25$ for each stage). (C,D) Visualization (C) and quantification (D) of GFP-tagged TF levels in the AC in relation to the division of P6.p. Brackets indicate 1° VPCs. Yellow and white arrowheads indicate the breach in the BM and ACs, respectively. In this and all other figures, circles and error bars denote mean±s.d. ($n \geq 25$ for each stage). A.U., arbitrary units; M.G.V., mean gray value. Scale bars: 5 µm.

generated TF-RNAi vectors quantitatively. We examined a minimum of 50 animals following targeted TF-RNAi depletions, collecting spinning disk confocal *z*-stacks using the same acquisition settings as used for the developmental series (Fig. 2B) in all experiments. Following image quantification, our results were consistent with the phenotypes identified in our original uterine-specific RNAi screen (Fig. 1, Fig. S3). However, by being able to quantify depletion of endogenous GFP-tagged TF targeted by RNAi, we were able to correlate phenotype with mRNA depletion more accurately. The *nhr-67* and *egl-43* improved RNAi constructs strongly knocked down their GFP-tagged endogenous targets, with depletions averaging 88% and 75%, respectively (Fig. S3E). This strong knockdown of *nhr-67* and *egl-43* was also correlated with highly penetrant AC invasion defects (61% and 100%, respectively). The completely penetrant defect from *egl-43(RNAi)* segregated into 26% of animals exhibiting a single AC that failed to invade and all other cases phenocopying loss of *nhr-67*, with multiple *cdh-3*-expressing non-invasive ACs (Fig. S3E). Depletion of *GFP::fos-1* by RNAi was also highly penetrant, with a mean depletion of 92% of GFP-tagged endogenous protein and 76% of treated animals with a defect in AC invasion (Fig. S3E). Although only loss of *hlh-2* prior to AC specification can affect AC fate directly resulting in zero ACs (Karp and Greenwald, 2004), *nhr-67* and *egl-43* also regulate the AC/VU decision (Hwang et al., 2007; Verghese et al., 2011). Thus, to ensure that the invasion defects we were observing were the result of post-AC specification defects following TF knockdown, we performed L2 platings and scored for invasion. Because L2 platings result in less time (~12 h at 25°C) exposed to TF-RNAi, we were not surprised to observe a lower penetrance of AC invasion defects compared with L1 platings targeting the other TFs (Fig. S3F). As all L2 platings phenocopied L1 platings, although at lower penetrance and with only depletion of *hlh-2* at the L1 stage directly affecting AC fate, we utilized L1 platings for their increased penetrance for *nhr-67*, *egl-43* and *fos-1* for the remainder of our experiments. Together, these results suggest that following strong TF depletion, loss of either *egl-43* or *hlh-2*

Development (2020) 147, dev185850. doi:10.1242/dev.185850

phenocopies *nhr-67* depletion, generating multiple, non-invasive ACs.

Identification of a feed-forward loop controlling NHR-67 activity

Next, we examined the relationship between the four pro-invasive TFs during invasion. To accomplish this, we performed a series of RNAi depletion experiments using synchronized L1 or L2 (for *hlh-2*) stage animals and quantified the amount of GFP-tagged endogenous TF in the AC in animals with defects in invasion at the P6.p four-cell stage. Whereas depletion of *fos-1* failed to significantly downregulate levels of *nhr-67::GFP*, depletion of *egl-43* resulted in a strong reduction (65%) of *nhr-67::GFP* in the AC (Fig. 3A,B). Intriguingly, in animals with a single non-invasive AC following *hlh-2(RNAi)* we saw only a partial reduction (19%) of *nhr-67::GFP* levels, whereas in animals with multiple *cdh-3*-expressing cells we saw a significant reduction (49%) in *nhr-67::GFP* (Fig. 5A,B). These results suggest that both *egl-43* and *hlh-2* co-regulate *nhr-67* during invasion.

We repeated these TF-RNAi molecular epistasis experiments with the remaining three TF-GFP-tagged strains and quantified depletion of GFP in animals with invasion defects. Consistent with previous studies using transcriptional and translational reporters (Hwang et al., 2007; Rimann and Hajnal, 2007), we found that depletion of *fos-1* regulated levels of *egl-43::GFP::egl-43* (44% depletion) (Fig. 3C,D). No other TF depletion significantly regulated the levels of *egl-43* in our experiments (Fig. 3C,D). *hlh-2* is predicted to regulate *egl-43* activity based on the presence of two conserved E-box binding motifs

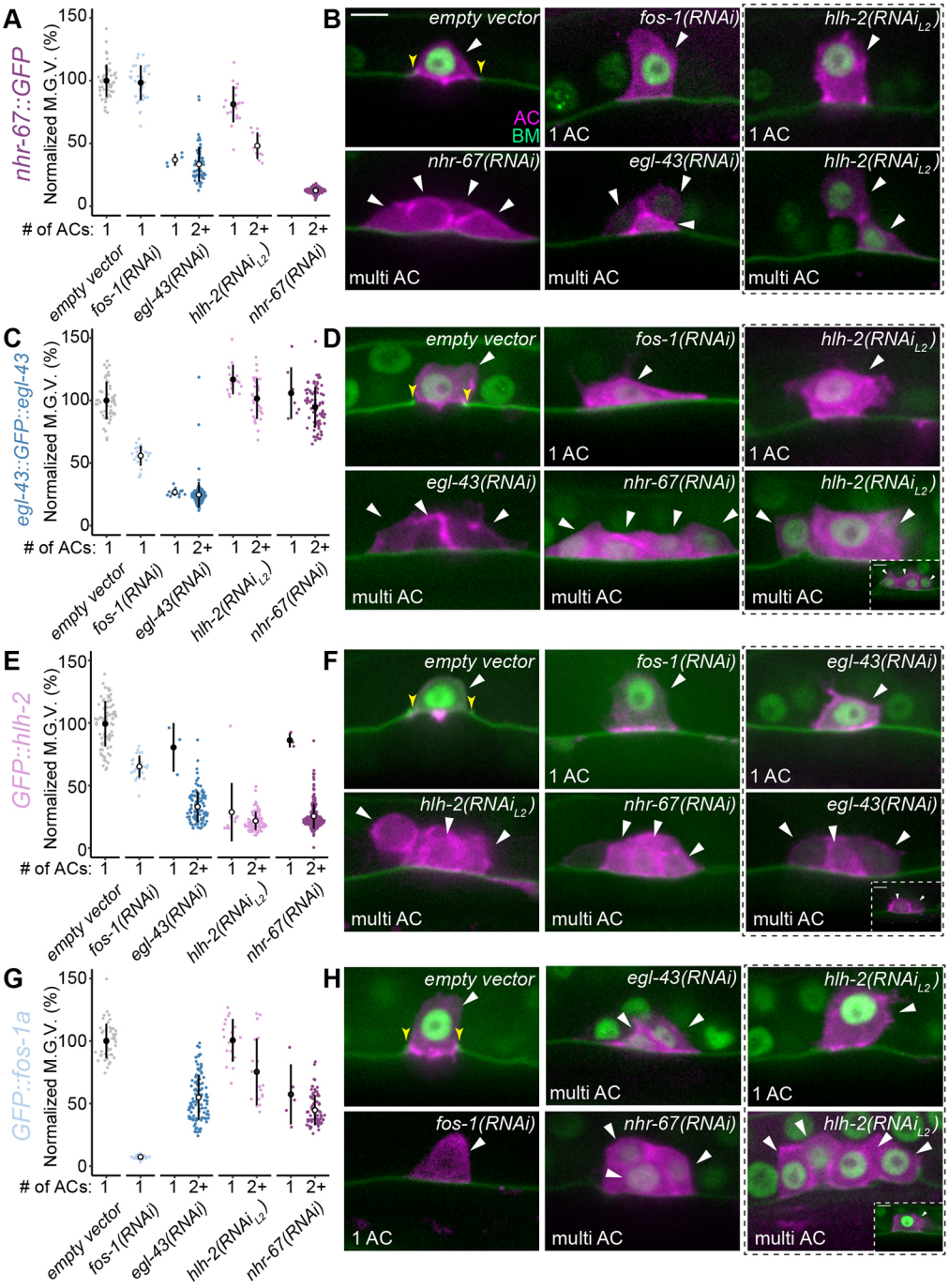

Fig. 3. Regulatory interactions among pro-invasive TFs at endogenous loci. (A,C,E,G) Sinaplots of GFP-tagged TF levels, defined as the mean gray value (M.G.V.) of individual AC nuclei, following RNAi perturbation ($n \geq 25$ animals per treatment, $P<1\times10^{-6}$, Student's *t*-test of TF-RNAi treated animals compared with empty vector). (B,D,F,H) Representative phenotypes (single versus multi AC, as noted bottom left of each image) following TF-RNAi depletion. Yellow and white arrowheads indicate the breach in the BM and ACs, respectively. Insets show additional ACs in other focal planes. Scale bars: 5 µm.

Development (2020) 147, dev185850. doi:10.1242/dev.185850

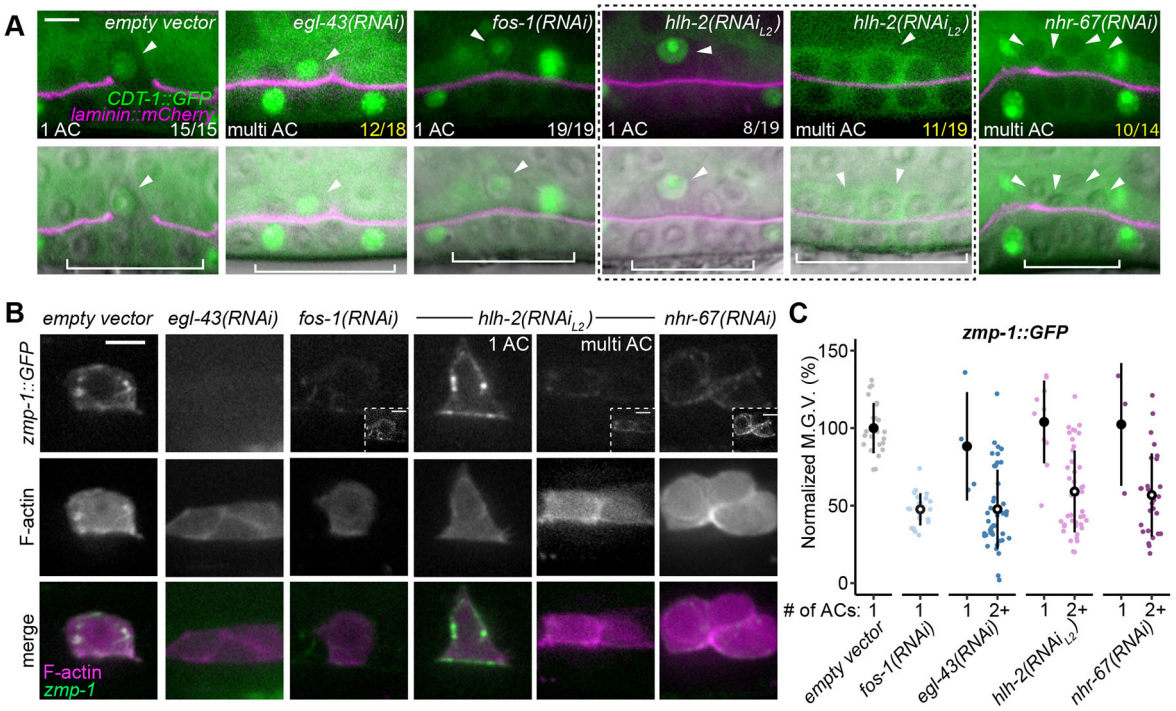

Fig. 4. Pro-invasive TFs regulate the cell cycle and MMPs. (A) Localization of the cell cycle state reporter *cdt-1*>CDT-1::GFP (green) and BM (*lam-1*>LAM-1::mCherry, magenta) in empty vector control (left) compared with TF-RNAi. White and yellow fractions (bottom right of each micrograph) indicate the number of animals exhibiting the phenotype shown. Brackets indicate 1° VPCs and arrowheads indicate ACs. Dashed box indicates single AC and multi-AC phenotypes resulting from *hlh-2* depletion. (B,C) Visualization (B) and quantification (C) of endogenous MMP (*zmp-1::GFP*) expression in individual ACs following RNAi perturbations ($n \geq 20$ animals per treatment, $P<0.01$, Student's *t*-test TF-RNAi treated animals compared with empty vector). Insets show additional ACs in different focal planes. M.G.V., mean gray value. Scale bars: 5 µm.

in the *egl-43* promoter (Hwang et al., 2007). However, we did not detect regulation of *egl-43::GFP::egl-43* in either the AC (Fig. 3C,D) or neighboring VU cells (Fig. S4). Next, we examined *GFP::hlh-2* levels following TF-RNAi depletions. Intriguingly, we found a similar pattern of regulation based on AC phenotype. Animals with single non-invasive ACs showed partial depletion of *GFP::hlh-2* following *fos-1*, *egl-43* or *nhr-67* depletion (35%, 20% and 14%, respectively). However, animals with multiple *cdh-3*-expressing ACs following *egl-43(RNAi)* or *nhr-67(RNAi)* showed stronger depletion of *GFP::hlh-2* (66% and 73%, respectively) (Fig. 3E,F). Finally, we examined levels of *GFP::fos-1* following TF depletions. Depletion of either *nhr-67* or *egl-43* resulted in partial reduction of *GFP::fos-1* levels in the AC (52% and 49%, respectively) (Fig. 3G,H). Together, these results suggest that *egl-43*, *hlh-2* and *nhr-67* may function together in a feed-forward regulatory loop with positive feedback to maintain the AC in a post-mitotic, pro-invasive state.

Multiple ACs derive from proliferation

As depletion of *egl-43* and *hlh-2* both regulate levels of *nhr-67* and their depletion results in multiple ACs that fail to invade, we next wanted to assess whether their depletion was functionally phenocopying depletion of *nhr-67*. To confirm that the presence of multiple cells expressing the *cdh-3*-driven AC reporter were due to defects in proliferation, we performed static imaging using a full-length translational *cdt-1*>CDT-1::GFP reporter that indicates cell cycle progression (Fig. 4A). As CDT-1 must be removed from origins of replication during DNA licensing, the transgene localizes to the nucleus during G1/G0 and is largely cytosolic at the onset of S phase (Matus et al., 2014, 2015). As expected, T444T (empty vector)- and *fos-1(RNAi)*-treated animals consistently exhibited nuclear localization of CDT-1::GFP [Fig. 4A; 100%, T444T, n=15; 100%, *fos-1(RNAi)*, n=19 animals examined], indicating cell cycle arrest. However, following depletion of *egl-43*, *hlh-2* and *nhr-67* we identified multiple animals (Fig. 4A) possessing non-invasive ACs lacking nuclear CDT-1::GFP, indicative of cycling ACs [67%, *egl-43(RNAi)*, n=12/18; 58%, *hlh-2(RNAi)*, n=11/19; 71%, *nhr-67(RNAi)*, n=10/14 animals examined]. Together, these results strongly support our molecular epistasis data suggesting that *egl-43* and *hlh-2* function upstream of *nhr-67* to maintain the post-mitotic state of the AC during invasion.

After examining the role of pro-invasive TFs in regulating cell cycle progression, we then sought to examine other downstream targets involved in AC invasion. Using an endogenously tagged GFP reporter for the MMP *zmp-1* (Kelley et al., 2019), we assessed the ability of ACs to produce MMPs following *TF(RNAi)* depletion. We confirmed previously published findings (Kelley et al., 2019) that *fos-1* depletion results in reduction of *zmp-1* expression (Fig. 4B). Interestingly, in the cases of the other *TF(RNAi)* treatments, a significant reduction of *zmp-1* expression was only observed when multiple *cdh-3*-expressing ACs were present (Fig. 4B), suggesting that cell cycle progression may downregulate production of MMPs.

EGL-43 and HLH-2 play roles in cell cycle-dependent and independent pathways

We have shown previously that the invasive activity of the AC following depletion of NHR-67 can be completely rescued by restoring the AC to a post-mitotic G1/G0 state through upregulation of the cyclin-dependent kinase inhibitor CKI-1 (p21/p27) (Matus et al., 2015). As our epistasis experiments revealed that *egl-43* and *hlh-2* positively co-regulate NHR-67 activity, we induced AC-specific expression of CKI-1 using a *cdh-3*>CKI-1::GFP integrated array and assessed invasion following RNAi depletions

Development (2020) 147, dev185850. doi:10.1242/dev.185850

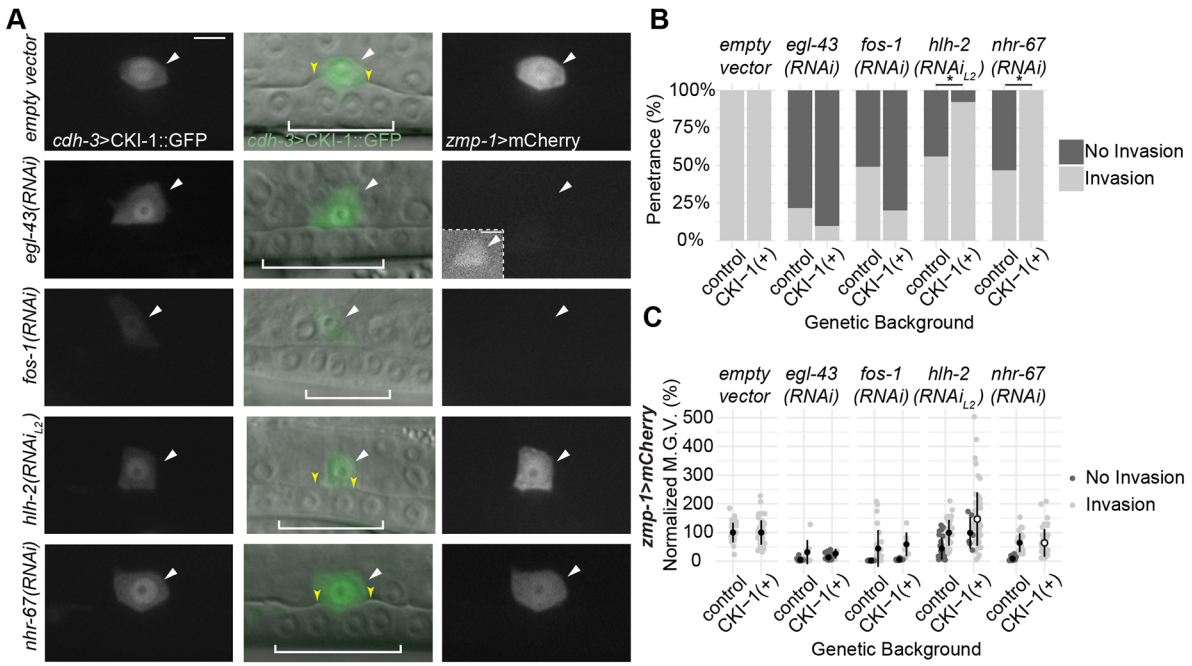

Fig. 5. HLH-2 depletion is partially rescued by induced G1/G0 arrest and EGL-43 has a cell cycle-independent pro-invasive role. (A) Micrographs depicting *cdh*-3>CKI-1::GFP (left), DIC overlay (middle), and *zmp-1*>mCherry expression (right) in empty vector control (top) and TF-RNAi depletions. Brackets indicate 1° VPCs. Yellow and white arrowheads indicate the breach in the BM and ACs, respectively. Inset shows the same image with enhanced exposure to show dim expression. Scale bars: 5 µm. (B) Quantification of AC invasion defects in control and CKI-1(+) animals ($n \geq 27$ animals per treatment, *$P<0.00001$, Fisher's exact test CKI-1(+) animals compared with those without the rescuing transgene). (C) Quantification of *zmp-1*>mCherry reporter levels in control and CKI-1(+) animals ($n \geq 27$ animals per treatment, $P<0.01$, Student's *t*-test CKI-1(+) animals compared with those without the rescuing transgene). M.G.V., mean gray value.

(Fig. 5A,B). As expected, induced expression of CKI-1::GFP in the AC completely rescued *nhr-67(RNAi)*-treated animals [Fig. 5A,B; 100% invaded (n=42) compared with 45% of control animals lacking induced CKI-1::GFP (n=62)]. Additionally, *cdh-3*>CKI-1::GFP partially rescued *hlh-2* depletion in L2 RNAi-feeding experiments by restoring AC invasion in most animals examined [Fig. 5A,B; 87% invaded (n=77), compared with 56% of control animals (n=59)]. Inducing G1/G0 arrest in the AC failed to rescue *fos-1(RNAi)*-treated animals [Fig. 5A,B; 20% invaded (n=35), compared with 51% of control animals (n=53)]. AC-specific expression of CKI-1::GFP blocked AC proliferation following *egl-43(RNAi)*; however, this induced arrest failed to rescue invasion [Fig. 5A,B; 10% invaded (n=31), compared with 19% of control animals (n=37)]. This result suggests that *egl-43* has pro-invasive functions outside of the cell cycle-dependent pathway. In support of a role for *egl-43* outside of cell cycle control, induced CKI-1::GFP restored the expression of a reporter of MMP activity (*zmp-1*>mCherry) in *nhr-67*-depleted animals, but neither *fos-1* nor *egl*-43-depleted animals showed restoration of *zmp-1* transcription (Fig. 5C). Together, these results reveal the presence of two integrated sub-circuits necessary for invasive activity, with *egl-43* and *hlh-2* likely having a crucial role in both circuits.

We next set out to test our putative network topology. To do this, we generated two new single copy transgenic lines expressing either BFP-tagged codon-optimized HLH-2 or the genomic region of NHR-67 under the transcriptional control of a heat shock promoter. Induced expression of HLH-2 failed to rescue AC invasion following depletion of *egl-43*, *fos-1* or *nhr-67*, consistent with *hlh-2* functioning upstream of *nhr-67* and the cell cycle-independent roles of *egl-43* and *fos-1* in regulating AC invasion (Fig. S5A). Similarly, induced expression of NHR-67 did not rescue invasion in *egl-43(RNAi)*- and *fos-1(RNAi)*-treated animals (Fig. S5B). Furthermore, induced expression of NHR-67 failed to rescue AC invasion in *hlh-2(RNAi)*-treated animals (Fig. S5B). This result, paired with the prevalence of single non-invasive ACs (Fig. 1C) and only partial rescue from induced CKI-1 (Fig. 5A,B) suggests that *hlh-2* regulates invasive targets independently of its role in regulating *nhr-67* and cell cycle arrest.

As our induced TF experiments failed to rescue invasion defects, we examined an *nhr-67* hypomorphic allele [*nhr-67(pf88)*], which we have previously shown results in an incomplete penetrance of mitotic, non-invasive ACs (Matus et al., 2015). Notably, *nhr-67(RNAi)* using the enhanced T444T vector did not significantly increase the invasion defect of the hypomorphic allele (Fig. S6), supporting previous results using the L4440-based *nhr-67* RNAi vector (Matus et al., 2015). Thus, the *nhr-67(pf88)* allele may represent a putative null phenotype for AC invasion. Similar to our results with *nhr-67(RNAi)*, depletion of *hlh-2* also failed to enhance the *nhr-67(pf88)* AC invasion defect significantly (Fig. S6). Together, these results suggest that *hlh-2* functions upstream of *nhr-67* in maintaining the AC in a post-mitotic, pro-invasive state.

EGL-43 isoforms function redundantly and in an autoregulative manner

Two functional isoforms of *egl-43* are encoded in the *C. elegans* genome (Fig. S7A). Previous research has suggested that the longer isoform functions downstream of *fos-1* to modulate MMP expression and other *fos-1* transcriptional targets, including *cdh-3* (Hwang et al., 2007; Rimann and Hajnal, 2007). The shorter isoform has been predicted to function in Notch/Delta-mediated AC specification and later Notch/Delta-mediated patterning of the ventral uterus (Hwang et al., 2007) or as a potential competitive inhibitor for long isoform binding of downstream targets (Rimann and Hajnal, 2007). Additionally, *fos-1* and *egl-43* have been shown to function in an incoherent feed-forward loop with negative feedback, with *fos-1*

Development (2020) 147, dev185850. doi:10.1242/dev.185850

positively regulating and *egl-43* negatively regulating the levels of *mig-10*/lamellipodin, a key adhesion protein important for stabilizing the attachment of the AC to the BM. Titrating levels of MIG-10 is crucial, as overexpression of MIG-10 results in AC invasion defects (Wang et al., 2014). Although it is readily apparent that levels of EGL-43 are also important, it is unclear from previous studies whether the two isoforms have divergent functions during invasion. Thus, we next decided to explore *egl-43* isoform function.

First, we generated a knock-in allele of GFP at the *egl-43* N-terminus to tag the long isoform (*GFP::egl-43L*) specifically. This allowed us to compare expression patterns of the long isoform to the internally GFP-tagged allele that should dually label both isoforms (Fig. S7A,B). We examined animals during uterine-vulval development and found overlapping expression patterns between both isoforms with strong expression throughout the somatic gonad (Fig. S7B). Next, we generated an *egl-43L*-specific improved RNAi targeting vector in T444T and examined *egl-43L* depletion in the uterine-specific RNAi-sensitive genetic background (Matus et al., 2010). Depletion of *egl-43L* resulted in a penetrant AC invasion defect, as expected, but, notably, we detected the presence of animals with both a single non-invasive AC (19%) and animals with multiple ACs (39%) (Fig. 6A,B), similar to depletion of both isoforms (Fig. 1C,E). We then assessed whether the long isoform has the same quantitative relationship to the other TFs as observed when targeting both isoforms. Indeed, *egl-43(RNAi)* and *egl-43L(RNAi)* exhibited comparable levels of depletion of *egl-43::GFP::egl-43* (75%, 78%), *GFP::hlh-2* (66%, 60%) and *nhr-67::GFP* (66%, 64%, respectively) ($n \geq 25$ animals examined per treatment) (Fig. S7C).

To characterize loss-of-function phenotypes further and examine transcriptional output of the two *egl-43* isoforms, we next examined endogenous transcriptional reporters that were created as an intermediate step in generating GFP knock-in alleles using the self-excising cassette (SEC) method (Dickinson and Goldstein 2016). Specifically, prior to Cre-Lox recombination, the insertion of GFP at the N-terminus of a locus with a ∼6 kb SEC generates a transcriptional reporter at the endogenous locus and often interferes with the native transcriptional machinery at the locus where it is inserted, generating a strong loss-of-function or putative null allele (Dickinson and Goldstein, 2016). Examination of pre-floxed versions of both edited knock-in alleles of *egl-43* was performed in the presence of an mT1 balancer, as homozygous animals are non-fertile. Similar to the putative null allele, *egl-43(tm1802)* (Rimann and Hajnal, 2007), the allele resulting from the SEC insertion of the internal GFP tag had an extremely low frequency of escapers, and we were unable to obtain L3-stage animals to examine for AC invasion defects. However, similar to our results with RNAi (Fig. 6A,B), an allele resulting from SEC insertion with the long isoform [*egl-43(bmd135)*] displayed a 31% AC invasion defect (n=11/36), with animals containing either single or multiple non-invading ACs (Fig. S7D,E). Finally, as previous reports based on transgenic transcriptional reporters have suggested that *egl-43* may be autoregulatory (Matus et al., 2010; Rimann and Hajnal, 2007; Wang et al., 2014), we examined the mT1-balanced pre-floxed allele of the internally tagged *egl-43* targeting both isoforms (*egl-43::GFP^SEC^::egl-43*). In support of these previous studies, we found strong evidence of autoregulation at the endogenous locus, as *egl-43(RNAi)* reduced the expression of GFP by 65% ($n \geq 25$ animals) (Fig. 6C,D). Taken together, these results suggest that both isoforms of *egl-43* function redundantly to regulate multiple transcriptional sub-circuits that are crucial for invasion.

Activation of the pro-invasive gene regulatory network occurs post-specification

Our results here identify a putative feed-forward loop between *egl-43*, *hlh-2* and *nhr-67* to maintain levels of NHR-67, which we have previously shown to be crucial for keeping the AC in a post-mitotic, pro-invasive state (Matus et al., 2015). As these same TFs also have been shown to function during the AC/VU decision (Hwang et al., 2007; Karp and Greenwald, 2004; Verghese et al., 2011), we investigated whether the same regulatory relationships were utilized during cell fate specification and invasion.

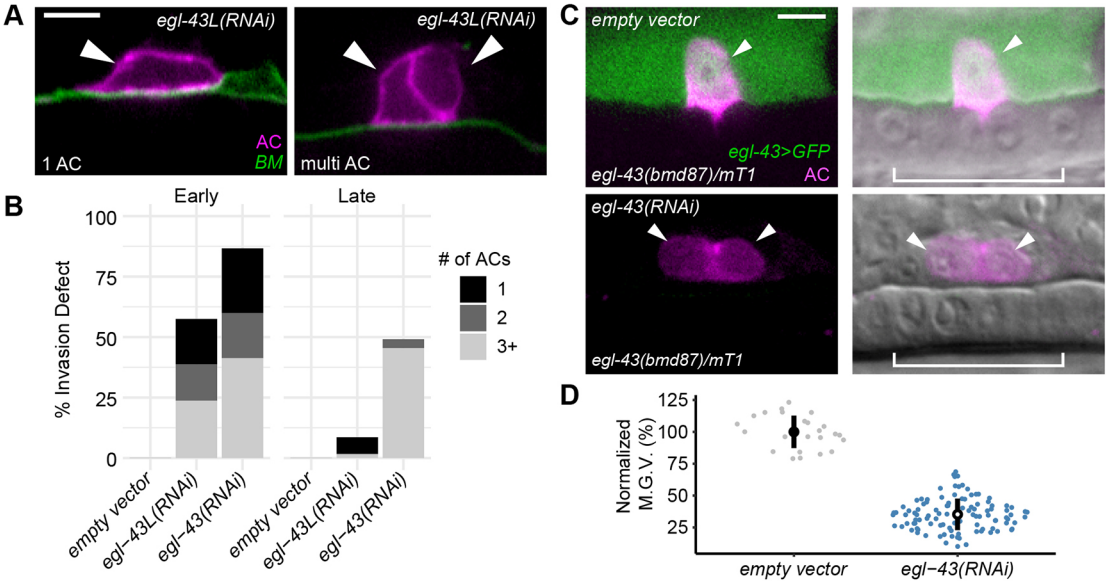

Fig. 6. Both isoforms of *egl-43* function redundantly to regulate AC invasion. (A,B) Visualization (A) and quantification (B) of AC invasion and proliferation defects resulting from RNAi depletion of the long isoform of *egl-43* (*egl-43L*). (C,D) Visualization (C) and quantification (D) of *egl-43*>GFP expression in individual AC nuclei, assessed using a balanced endogenous *egl-43* transcriptional reporter [*egl-43(bmd87)/mT1*], following *egl-43(RNAi)* treatment compared with control ($n \geq 25$ animals per treatment, $P<1\times10^{-15}$, Student's *t*-test). Arrowheads and brackets indicate ACs and 1° VPCs, respectively. M.G.V., mean gray value. Scale bars: 5 µm.

Development (2020) 147, dev185850. doi:10.1242/dev.185850

Intriguingly, our examination of TF onset establishes a hierarchy of *egl-43*, *hlh-2* and *nhr-67* reaching steady-state levels in the descendants of Z1 and Z4, although all three TFs are robustly expressed in the AC/VU cells (Fig. 2A). To examine TF regulatory relationships prior to specification, we performed L1 TF RNAi platings and determined expression levels of TF-GFP in the AC/VU cells in L2-stage animals. Although each TF RNAi robustly depleted its target GFP allele, we failed to detect any molecular epistatic interactions between TFs in the AC/VU cells (Fig. 7A,B). In support of previous research demonstrating a role for these TFs in regulating the AC/VU decision (Hwang et al., 2007; Karp and Greenwald, 2004; Verghese et al., 2011), we detected significant depletion of an endogenously GFP-tagged allele of *lin-12* (Notch) (Fig. 7C,D). Together, these results suggest that, despite the re-iterative use of the same set of TFs in specification and invasion, the gene regulatory network (GRN) we characterized here is specific for the post-specification pro-invasive behavior of the AC.

DISCUSSION

Cellular invasion requires coordination of extrinsic cues from the surrounding microenvironment and orchestration of intrinsic regulatory circuits (Sherwood and Plastino, 2018). We focus here on exploring the intrinsic pathways that autonomously regulate *C. elegans* AC invasion. Combining improved RNAi targeting vectors with GFP-tagged alleles enabled us to correlate phenotype with depletion of the endogenous mRNAs and compare regulatory relationships in a quantitative framework. Our experiments reveal new roles for *egl-43* and *hlh-2* in regulating *nhr-67*-mediated cell cycle arrest and suggest that these TFs function in a coherent feed-forward loop with positive feedback. Additionally, we confirm previous work demonstrating that *egl-43* is autoregulatory and demonstrate that it functions in both the cell cycle-dependent sub-circuit as well as in a cell cycle-independent manner, through *fos-1*, to orchestrate invasion (Fig. 8). Together, building upon previous work using transgenic approaches (Bodofsky et al., 2018; Hwang et al., 2007; Rimann and Hajnal, 2007; Schindler and Sherwood, 2011; Verghese et al., 2011), our results using endogenously tagged alleles provide the first description of the native regulatory relationships between the four TFs that promote invasion during *C. elegans* uterine-vulval attachment.

A key function of *nhr-67* is to maintain the post-mitotic state of the AC (Matus et al., 2015). Here, we demonstrate that *egl-43* and

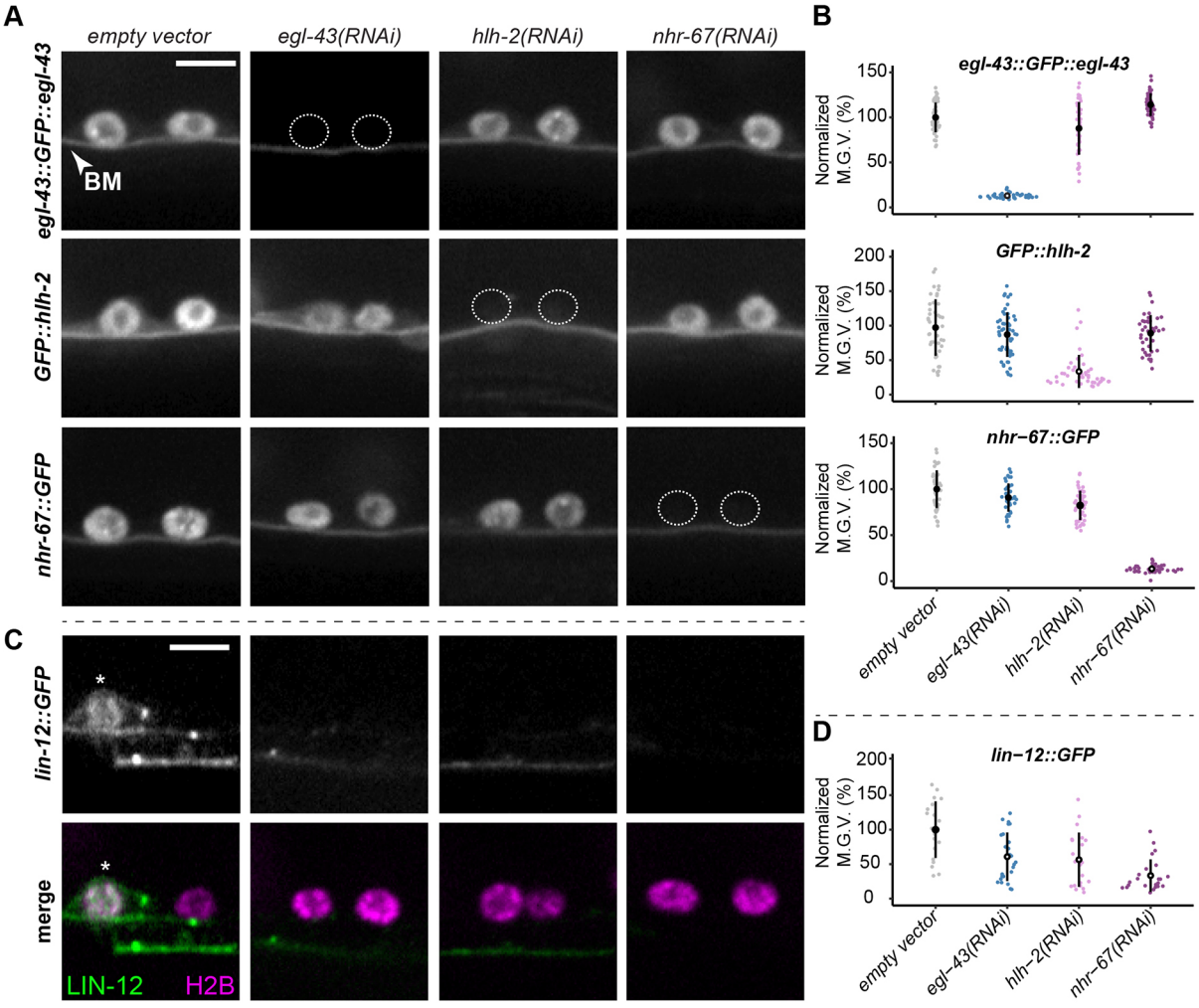

Fig. 7. Regulatory relationships do not exist prior to AC specification. (A,B) Visualization (A) and quantification (B) of GFP-tagged TF levels in the AC/VU precursors (Z1.ppp and Z4.aaa) following RNAi perturbations ($n \geq 20$ animals per treatment, $P < 1 \times 10^{-6}$, Student's *t*-test TF-RNAi treated animals compared with empty vector). Dashed circles indicated location of AC/VU precursor cells in experiments where TF::GFP is strongly depleted by the targeting RNAi. (C,D) Visualization (C) and quantification (D) of GFP-tagged *lin-12* (asterisks) in the AC/VU precursors following RNAi perturbations ($n \geq 20$ animals per treatment, $P < 0.01$, Student's *t*-test TF-RNAi treated animals compared with empty vector). M.G.V., mean gray value. Scale bars: 5 µm.

Development (2020) 147, dev185850. doi:10.1242/dev.185850

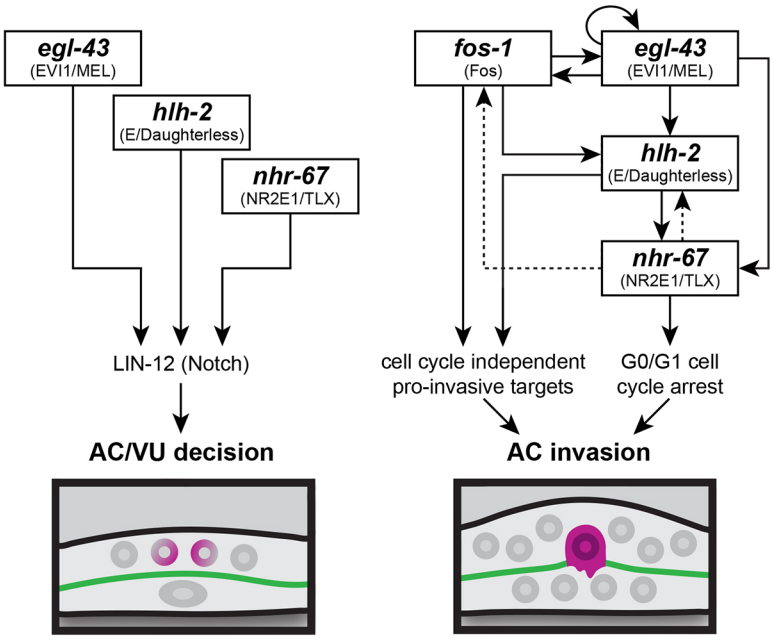

Fig. 8. Summary model of the GRNs coordinating AC specification and invasion. Left: the Notch-mediated AC/VU cell fate decision appears to be independently regulated by *egl-43*, *hlh-2* and *nhr-67*. Right: network inference predicts that the GRN regulating AC invasion contains cell cycle-independent and -dependent sub-circuits, the latter entailing a type I coherent feed-forward loop with positive feedback to maintain the AC in a post-mitotic, invasive state. Dotted lines represent predicted feedback.

hlh-2 both regulate *nhr-67*, and that *nhr-67*-depletion also reduces HLH-2 levels. Network inference suggests these three TFs function in a classic type I coherent feed-forward loop regulatory circuit with positive feedback (Mangan and Alon, 2003) (Fig. 8). Our model fits with data by others showing that *hlh-2* may directly bind to the *nhr-67* promoter through two canonical E-box motifs found in a 164 bp window in a functional promoter element deleted in several hypomorphic alleles of *nhr-67* (Bodofsky et al., 2018; Matus et al., 2015; Verghese et al., 2011). Further, deletion of these *hlh-2* conserved binding sites results in loss of AC-specific GFP expression in transgenic lines (Bodofsky et al., 2018). Although others have also reported positive regulation by EGL-43 on *nhr-67* activity via transgenic reporters (Bodofsky et al., 2018), this interaction, and many of the other TF interactions, may be indirect, as no known binding sites exist for EGL-43 in the *nhr-67* promoter. Alternatively, EGL-43 and NHR-67 have been predicted, based on yeast two-hybrid experiments, to interact at the protein-protein level (Reece-Hoyes et al., 2013).

We have also examined the activity of the two previously identified isoforms of *egl-43* (Hwang et al., 2007; Rimann and Hajnal, 2007). As both mutant analyses and RNAi depletion of the long isoform phenocopy depletion of both isoforms, our data suggest that either the long isoform of *egl-43* functions redundantly with the short isoform or it functions as the dominant isoform at the intersection of multiple regulatory circuits. Of these two possible hypotheses, the latter is supported by a recent report demonstrating that the long isoform of *egl-43* is a key upstream regulator of the post-mitotic state of the AC as mutation of the transcriptional start methionine of the short isoform of *egl-43* has no observable AC invasion defect and an AC-specific genetic knockout of the long isoform results in mitotic, non-invasive ACs (Deng et al., 2019 preprint).

Together, our data and corroborating evidence from the literature support the existence of a coherent feed-forward circuit with positive feedback among *egl-43*, *hlh-2* and *nhr-67* in maintaining the post-mitotic state of the AC (Fig. 8). We have previously shown that *nhr-67* positively regulates transcripts of *cki-1* specifically in the AC (Matus et al., 2015). Thus, to test our putative regulatory circuit, we induced expression of *cki-1* in the AC, which prevents the AC from inappropriately entering the cell cycle. This forced G1/G0 arrest fully rescues *nhr-67* depletion (Matus et al., 2015). Induced *cki-1* partially rescued *hlh-2* depletion but failed to rescue *egl-43* depletion. Heat shock-induced expression of *nhr-67* failed to rescue either *hlh-2* or *egl-43*, suggesting that *hlh-2*, like *egl-43*, has a cell cycle-independent function. These results suggest that *egl-43* and *hlh-2* function in multiple regulatory circuits. For *egl-43*, this is supported by recent work demonstrating a type I incoherent feed-forward loop between *fos-1*, *egl-43L* and the BM adhesion protein MIG-10/lamellipodin (Wang et al., 2014). Finally, our observation that *egl-43* is autoregulatory, also shown previously by promoter>GFP fusion experiments (Matus et al., 2015; Rimann and Hajnal, 2007; Wang et al., 2014), supports a model in which *egl-43* occupies a key node at the intersection of multiple pro-invasive circuits (Fig. 8).

Feed-forward regulatory loops are likely the most well-described network motif occurring in all GRNs (Cordero and Hogeweg, 2006; Davidson, 2010; Mangan and Alon, 2003). From *E. coli* (Shen-Orr et al., 2002) and yeast (Lee et al., 2002; Milo et al., 2002) to a myriad of examples across the Metazoa (reviewed by Davidson, 2010), feed-forward loops are thought to function as filters for transient inputs (reviewed by Alon, 2007; Hinman, 2016). The addition of positive feedback, generating a coherent feed-forward loop, provides stability to a sub-circuit and is often found in differentiation gene batteries coincident with autoregulation (Davidson, 2010). These network motifs have been described in many developmental contexts, including MyoD-driven vertebrate skeletal muscle differentiation (Penn et al., 2004), patterning of the *Drosophila* egg shell via the TF Broad and interactions with EGFR and Dpp signaling (Yakoby et al., 2007), Pax6-dependent regulation of Maf and crystallin expression in the mouse embryonic lens (Xie and Cvekl, 2011) and terminal selector neuronal differentiation in *C. elegans* and mammals (reviewed by Hobert, 2008). During *C. elegans* embryonic development, a series of coherent feed-forward loops utilizing SKN-1/MED-1,2 and then a suite of reiteratively used GATA factors (END-1,-3) are required to pattern endomesoderm development successfully (reviewed by Maduro, 2009). Thus, the coherent feed-forward loop identified here maintaining the post-mitotic state in the *C. elegans* AC likely evolved to coordinate AC cell cycle exit, both as a by-product of terminal differentiation and a morphogenetic requirement for invasive behavior (Matus et al., 2015). AC invasion is necessary for egg laying,

Development (2020) 147, dev185850. doi:10.1242/dev.185850

and defects in the process results in penetrant Protruding vulva/Egg-laying defective (Pvl/Egl) phenotypes, reducing fecundity in individual animals by nearly ten-fold. Thus, redundant control of the sub-circuit regulating invasion and cell cycle arrest may have been under strong selection, providing an explanation for the regulatory relationships between *egl-43*, *hlh-2* and *nhr-67* we characterize here.

As *egl-43*, *hlh-2* and *nhr-67* reach steady-state levels prior to the time of AC/VU specification and individually have been previously shown to regulate different aspects of the stochastic cell fate decision between the AC and VU (Hwang et al., 2007; Karp and Greenwald, 2004; Verghese et al., 2011), we performed RNAi depletion experiments and examined TF::GFP levels in the AC/VU cells during the L2 stage. Surprisingly, we found no evidence of regulation between the TFs at this stage, though, as expected, all three TFs regulated levels of endogenously tagged *lin-12::GFP* (Notch). This suggests that the feed-forward loop functions specifically in the post-specification AC to maintain the post-mitotic, invasive state (Fig. 8). Transient TF-DNA binding and GRN rewiring can result from responses to diverse stimuli (Luscombe et al., 2004; Swift and Coruzzi, 2017). One plausible explanation for this temporal change in network topology is that cell cycle-dependent changes in chromatin remodeling and TF activity likely changes the genomic landscape between the bipotential AC/VU cells and the post-mitotic, differentiated AC (Ma et al., 2015). Additionally, there may be differentially expressed co-factor(s) functioning during specification or invasion that facilitate interactions between TFs. Reiterative use of the same TFs to program different cell behaviors has been examined during neuronal differentiation (Guillemot, 2007) and neural crest specification and migration, as the winged-helix TF FoxD3 was recently shown to regulate multiple independent chromatin-organizing circuits, functioning as a pioneer factor during zebrafish neural crest specification and a transcriptional repressor during later events, including epithelial-mesenchymal transition and migration (Lukoseviciute et al., 2018). Whether or not *egl-43*, *nhr-67* or *hlh-2* function as pioneer factors during AC/VU specification is an open question, and one that could soon be tackled through isolation by fluorescence-activated cell sorting and the application of newer next-generation sequencing tools such as ATAC-seq (assay for transposase-accessible chromatin using sequencing) or CUT&RUN (cleavage under targets and release using nuclease) (Skene and Henikoff, 2017).

We are just beginning to understand the connections between regulatory circuits and morphogenetic behaviors (Christiaen et al., 2008; Martik and McClay, 2015; Saunders and McClay, 2014). Hopefully, the ease of genome editing and protein perturbation strategies will facilitate the kind of analyses we have performed here in other metazoan systems. In summary, in this study we characterize the complex relationships between the four pro-invasive TFs that function in the AC to program invasive behavior. We show that although the TFs are reiteratively used in both cell fate specification and in a differentiated cell behavior, invasion, they only interact with each other following specification. We identify a classic type I feed-forward loop regulating mitotic exit and controlling a switch between proliferative and invasive behavior. Whether or not similar circuit architecture is utilized to regulate invasive and proliferative cell biology in other developmental invasive contexts, including mammalian trophoblast implantation and placentation (Carter et al., 2015; Red-Horse et al., 2004) and epithelial to mesenchymal transition events during gastrulation (Vega et al., 2004), is still poorly understood. Finally, as there appear to be many cancer subtypes that may switch between proliferative and invasive fates (reviewed by Kohrman and Matus, 2017), improving our understanding of the GRN architecture of invasive cells may provide new therapeutic nodes to target in reducing the lethality associated with cancer metastasis.

MATERIALS AND METHODS

C. elegans strains and culture conditions

Animals were reared under standard conditions and cultured at 25°C, with the exception of temperature-sensitive strains including those containing heat shock-inducible transgenes or the *rrf-3(pk1426)* allele (conferring RNAi hypersensitivity), which were maintained at 15°C and 20°C (Brenner, 1974; Simmer et al., 2002). Heat shock-inducible transgenes were activated by incubating animals on plates at 32°C for 1 h following AC specification and again just prior to AC invasion. Animals were synchronized for experiments through alkaline hypochlorite treatment of gravid adults to isolate eggs (Porta-de-la-Riva et al., 2012). In the text and figures, we designate linkage to a promoter through the use of the>symbol and fusion of a proteins by a :: annotation. The following transgenes and alleles were used in this study: *qyIs102[fos-1>RDE-1;myo-2>YFP]* **LG I** *hlh-2(bmd90[hlh-2>LoxP::GFP::HLH-2])*, *qyIs227[cdh-3>mCherry::moeABD]*, *bmd121[LoxP::hsp>NHR-67::2xBFP]*, *bmd142[hsp>HLH-2::2xBFP]*; **LG II** *egl-43(bmd87[egl-43>SEC::GFP::EGL-43])*, *egl-43(bmd88[egl-43>LoxP::GFP::EGL-43])*, *egl-43(bmd136[egl-43L>LoxP::GFP::EGL-43])* *rrf-3(pk1426)*; *qyIs17[zmp-1>mCherry]* **LG III** *unc-119(ed4)*, **LG IV** *nhr-67(syb509[nhr-67>NHR-67::GFP])*, *qyIs10[lam-1>LAM-1::GFP]* **LG V** *fos-1(bmd138[fos-1>LoxP::GFP::FOS-1])*, *qyIs225[cdh-3>mCherry::moeABD]*, *rde-1(ne219)*, *qyIs24[cdh-3$^{1.5}$>mCherry::PLCδPH]*, *qyIs266[cdh-3>CKI-1::GFP]* **LG X** *qyIs7[lam-1>LAM-1::GFP]*. See Table S3 for additional details of strains used and generated in this study.

Molecular biology and microinjection

TFs were tagged at their endogenous loci using CRISPR/Cas9 genome editing via microinjection into the hermaphrodite gonad (Dickinson and Goldstein, 2016; Dickinson et al., 2013). Repair templates were generated as synthetic DNAs from either Integrated DNA Technologies (IDT) as gBlocks or Twist Biosciences as DNA fragments and cloned into *ccdB* compatible sites in pDD282 by New England Biolabs Gibson assembly (Dickinson et al., 2015). Homology arms ranged from 690 to 1200 bp (see Tables S4-S6 for additional details). sgRNAs were constructed by EcoRV and NheI digestion of the plasmid pDD122. A 230 bp amplicon was generated replacing the sgRNA targeting sequence from pDD122 with a new sgRNA, and NEB Gibson assembly was used to generate new sgRNA plasmids (see Tables S4-S6 for additional details). Hermaphrodite adults were co-injected with guide plasmid (50 ng/µl), repair plasmid (50 ng/µl) and an extrachromosomal array marker (pCFJ90, 2.5 ng/µl), and incubated at 25°C for several days before carrying out screening and floxing protocols associated with the SEC system (Dickinson et al., 2015).

RNA interference

An RNAi library of the pro-invasive TFs was constructed by cloning 950-1000 bp of synthetic DNA (663 bp for the *egl-43* long-specific isoform) based on cDNA sequences available on WormBase (www.wormbase.org) into the highly efficient T444T RNAi vector (Grove et al., 2018; Sturm et al., 2018). Synthetic DNAs were generated by IDT as gBlocks or Twist Biosciences as DNA fragments and cloned into restriction-digested T444T using NEB Gibson Assembly (see Tables S4, S5 and S7 for additional details). For most experiments, synchronized L1-stage animals were directly exposed to RNAi through feeding with bacteria expressing dsRNA (Conte et al., 2015). Because early *hlh-2* RNAi treatment perturbs AC specification, animals were initially placed on empty vector RNAi plates and then transferred to *hlh-2* RNAi plates following AC specification, approximately 12 h later at 25°C or 24 h later at 15°C (Schindler and Sherwood, 2011).

Live-cell imaging

All micrographs included in this manuscript were collected on a Hamamatsu Orca EM-CCD camera mounted on an upright Zeiss AxioImager A2 with a Borealis-modified CSU10 Yokagawa spinning disk scan head (Nobska Imaging) using 488 nm and 561 nm Vortran lasers in a VersaLase merge

and a Plan-Apochromat 100×/1.4 (NA) Oil DIC objective. MetaMorph software (Molecular Devices) was used for microscopy automation. Several experiments were scored using epifluorescence visualized on a Zeiss Axiocam MRM camera, also mounted on an upright Zeiss AxioImager A2 and a Plan-Apochromat 100×/1.4 (NA) Oil DIC objective. Animals were mounted into a drop of M9 on a 5% Noble agar pad containing approximately 10 mM sodium azide anesthetic and topped with a coverslip.

Scoring of AC invasion

AC invasion was scored at the P6.p four-cell stage, when 100% of wild-type animals exhibit a breached BM (Sherwood and Sternberg, 2003). Presence of green fluorescence under the AC, in strains with the laminin::GFP transgene, or presence of a phase dense line, in strains without the transgene, was used to assess invasion. Wild-type invasion is defined as a breach as wide as the basolateral surface of the AC, whereas partial invasion indicates the presence of a breach smaller than the footprint of the AC (Sherwood and Sternberg, 2003). Raw scoring data is available in Tables S1 and S2.

Image quantification and statistical analyses

Images were processed using Fiji/ImageJ (v.1.52q) (Schindelin et al., 2012). Expression levels of TFs were measured by quantifying the mean gray value of AC nuclei, defined as somatic gonad cells strongly expressing the *cdh-3>mCherry::moeABD* transgene, subtracting the mean gray value of a background region of an equal area to account for EM-CCD camera noise, which we use as a proxy for background fluorescence, as measurements of the mean gray value of unlabeled ACs approximately correspond to camera noise (means=2514.2 and 2243.5, respectively). Levels of *zmp-1*>mCherry were quantified in control and *cdh-3*>CKI-1::GFP animals by measuring the mean gray value of the entire AC, selected either by a hand-drawn region of interest or using the threshold and wand tools in Fiji/ImageJ. For characterization of downstream targets (Fig. 4) and molecular epistasis experiments (Fig. 3, Figs S3 and S7) at the L3 stage, only TF-RNAi animals exhibiting defects in invasion were included in the analysis. Data was normalized to negative control (empty vector) values for the plots in Figs 3-7 and Figs S5-S7, and to both negative control and positive control values for determining the interaction strengths represented in Fig. 8. Images were overlaid and figures were assembled using Adobe Photoshop (v. 20.0.6) and Illustrator CS (v. 10.14), respectively. Statistical analyses and plotting of data were conducted using RStudio (v. 1.1.463). Individual data points for each experiment were collected over multiple days. Statistical significance was determined using either a two-tailed Student's *t*-test or Fisher's exact probability test. Figure legends specify when each test was used and the *P*-value cut-off.

Acknowledgements

We are grateful to R. Adikes, B. Kinney, A. Kohrman, M. Martinez and B. Martin for comments on the manuscript. We also thank I. Greenwald for providing the endogenously tagged *lin-12*>LIN-12::GFP strain used in Fig. 7C. Some strains were provided by the *Caenorhabditis* Genetics Center, which is funded by the NIH Office of Research Infrastructure Programs [P40 OD010440].

Competing interests

The authors declare no competing or financial interests.

Author contributions

Conceptualization: T.N.M., D.Q.M.; Methodology: T.N.M., D.Q.M.; Validation: T.N.M., D.Q.M.; Formal analysis: T.N.M., J.J.S., N.J.P., D.Q.M.; Investigation: T.N.M., J.J.S., N.J.P., D.Q.M.; Resources: T.N.M., J.J.S., N.J.P., S.T., W.Z., D.Q.M.; Data curation: T.N.M., J.J.S., D.Q.M.; Writing - original draft: T.N.M., D.Q.M.; Writing - review & editing: T.N.M., J.J.S., N.J.P., D.Q.M.; Visualization: T.N.M., J.J.S., N.J.P., D.Q.M.; Supervision: W.Z., D.Q.M.; Project administration: D.Q.M.; Funding acquisition: D.Q.M.

Funding

This work was funded by the National Institutes of Health (NIH) National Cancer Institute [5R00CA154870-05 to D.Q.M.] and National Institute of General Medical Sciences (NIGMS) [1R01GM121597-01 to D.Q.M.]. D.Q.M. is also a Damon Runyon-Rachleff Innovator supported (in part) by the Damon Runyon Cancer Research Foundation [DRR-47-17]. T.N.M.-K. is supported by the NIH Eunice Kennedy Shriver National Institute of Child Health and Human Development [F31HD100091-01]. J.J.S. is supported by NIGMS [3R01GM121597-02S1] and N.J.P. is supported by the American Cancer Society [132969-PF-18-226-01-CSM]. Deposited in PMC for release after 12 months.

Supplementary information

Supplementary information available online at
http://dev.biologists.org/lookup/doi/10.1242/dev.185850.supplemental

References

Alon, U. (2007). Network motifs: theory and experimental approaches. *Nat. Rev. Genet.* **8**, 450-461. doi:10.1038/nrg2102

Attner, M. A., Keil, W., Benavidez, J. M. and Greenwald, I. (2019). HLH-2/E2A expression links stochastic and deterministic elements of a cell fate decision during *C. elegans* gonadogenesis. *Curr. Biol.* **29**, 3094-3100. doi:10.1016/j.cub.2019.07.062

Bodofsky, S., Liberatore, K., Pioppo, L., Lapadula, D., Thompson, L., Birnbaum, S., McClung, G., Kartik, A., Clever, S. and Wightman, B. (2018). A tissue-specific enhancer of the *C. elegans* nhr-67/tailless gene drives coordinated expression in uterine stem cells and the differentiated anchor cell. *Gene Expr. Patterns* **30**, 71-81. doi:10.1016/j.gep.2018.10.003

Brenner, S. (1974). The genetics of *Caenorabditis elegans*. *Genetics* **77**, 71-94.

Carter, A. M., Enders, A. C. and Pijnenborg, R. (2015). The role of invasive trophoblast in implantation and placentation of primates. *Philos. Trans. R. Soc. B Biol. Sci.* **370**, 20140070-20140070. doi:10.1098/rstb.2014.0070

Christiaen, L., Davidson, B., Kawashima, T., Powell, W., Nolla, H., Vranizan, K. and Levine, M. (2008). The transcription/migration interface in heart precursors of *Ciona intestinalis*. *Science* **320**, 1349-1352. doi:10.1126/science.1158170

Conte, D., Jr., MacNeil, L. T., Walhout, A. J. M. and Mello, C. C. (2015). RNA interference in *Caenorhabditis Elegans*. *Curr. Protoc. Mol. Biol.* **109**, 26.3.1-26.3.30. doi:10.1002/0471142727.mb2603s109

Cordero, O. X. and Hogeweg, P. (2006). Feed-forward loop circuits as a side effect of genome evolution. *Mol. Biol. Evol.* **23**, 1931-1936. doi:10.1093/molbev/msl060

Davidson, E. H. (2010). Emerging properties of animal gene regulatory networks. *Nature* **468**, 911-920. doi:10.1038/nature09645

Deng, T., Daube, M., Hajnal, A. and Lattmann, E. (2019). The *C. elegans* homolog of the Evi1 proto-oncogene, egl-43, coordinates G1 cell cycle arrest with pro-invasive gene expression during anchor cell invasion. *bioRxiv*, 1-37. doi:10.1101/802355

Dickinson, D. J. and Goldstein, B. (2016). CRISPR-based methods for *Caenorhabditis Elegans* genome engineering. *Genetics* **202**, 885-901. doi:10.1534/genetics.115.182162

Dickinson, D. J., Ward, J. D., Reiner, D. J. and Goldstein, B. (2013). Engineering the *Caenorhabditis elegans* genome using Cas9-triggered homologous recombination. *Nat. Methods* **10**, 1028-1034. doi:10.1038/nmeth.2641

Dickinson, D. J., Pani, A. M., Heppert, J. K., Higgins, C. D. and Goldstein, B. (2015). Streamlined genome engineering with a self-excising drug selection cassette. *Genetics* **200**, 1035-1049. doi:10.1534/genetics.115.178335

Grove, C., Cain, S., Chen, W. J., Davis, P., Harris, T., Howe, K. L., Kishore, R., Lee, R., Paulini, M., Raciti, D. et al. (2018). Using WormBase: a genome biology resource for *Caenorhabditis elegans* and related nematodes. *Methods Mol. Biol.* **1757**, 399-470. doi:10.1007/978-1-4939-7737-6_14

Guillemot, F. (2007). Spatial and temporal specification of neural fates by transcription factor codes. *Development* **134**, 3771-3780. doi:10.1242/dev.006379

Haerty, W., Artieri, C., Khezri, N., Singh, R. S. and Gupta, B. P. (2008). Comparative analysis of function and interaction of transcription factors in nematodes: Extensive conservation of orthology coupled to rapid sequence evolution. *BMC Genomics* **9**, 1-16. doi:10.1186/1471-2164-9-399

Hagedorn, E. J., Yashiro, H., Ziel, J. W., Ihara, S., Wang, Z. and Sherwood, D. R. (2009). Integrin acts upstream of Netrin signaling to regulate formation of the anchor cell's invasive membrane in C. elegans. *Dev. Cell* **17**, 187-198. doi:10.1016/j.devcel.2009.06.006

Hagedorn, E. J., Ziel, J. W., Morrissey, M. A., Linden, L. M., Wang, Z., Chi, Q., Johnson, S. A. and Sherwood, D. R. (2013). The netrin receptor DCC focuses invadopodia-driven basement membrane transmigration in vivo. *J. Cell Biol.* **201**, 903-913. doi:10.1083/jcb.201301091

Hanahan, D. and Weinberg, R. A. (2011). Hallmarks of cancer: the next generation. *Cell* **144**, 646-674. doi:10.1016/j.cell.2011.02.013

Hinman, V. F. (2016). Conservation and evolution of gene networks driving development. *Encycl. Evol. Biol.* 110-116. doi:10.1016/B978-0-12-800049-6.00130-X

Hobert, O. (2008). Regulatory logic of neuronal diversity: terminal selector genes and selector motifs. *Proc. Natl. Acad. Sci. USA* **105**, 20067-20071. doi:10.1073/pnas.0806070105

Hwang, B. J., Meruelo, A. D. and Sternberg, P. W. (2007). *C. elegans* EVI1 proto-oncogene, EGL-43, is necessary for Notch-mediated cell fate specification and regulates cell invasion. *Development* **134**, 669-679. doi:10.1242/dev.02769

Karp, X. and Greenwald, I. (2004). Multiple roles for the E/Daughterless ortholog HLH-2 during *C. elegans* gonadogenesis. *Dev. Biol.* **272**, 460-469. doi:10.1016/j.ydbio.2004.05.015

Kelley, L. C., Lohmer, L. L., Hagedorn, E. J. and Sherwood, D. R. (2014). Traversing the basement membrane in vivo: A diversity of strategies. *J. Cell Biol.* **204**, 291-302. doi:10.1083/jcb.201311112

Kelley, L. C., Chi, Q., Cáceres, R., Hastie, E., Schindler, A. J., Jiang, Y., Matus, D. Q., Plastino, J. and Sherwood, D. R. (2019). Adaptive F-actin polymerization and localized ATP production drive basement membrane invasion in the absence of MMPs. *Dev. Cell* **48**, 313-328.e8. doi:10.1016/j.devcel.2018.12.018

Kim, H., Ishidate, T., Ghanta, K. S., Seth, M., Conte, D., Shirayama, M. and Mello, C. C. (2014). A Co-CRISPR strategy for efficient genome editing in Caenorhabditis elegans. *Genetics* **197**, 1069-1080. doi:10.1534/genetics.114.166389

Kimble, J. and Hirsh, D. (1979). The postembryonic cell lineages of the hermaphrodite and male gonads in *Caenorhabditis elegans*. *Dev. Biol.* **70**, 396-417. doi:10.1016/0012-1606(79)90035-6

Kohrman, A. Q. and Matus, D. Q. (2017). Divide or conquer: cell cycle regulation of invasive behavior. *Trends Cell Biol.* **27**, 12-25. doi:10.1016/j.tcb.2016.08.003

Lee, T. I., Hannett, N., Harbison, C., Thompson, C., Simon, I., Zeitlinger, J., Jennings, E., Murray, H., Gordon, D., Ren, B. et al. (2002). Transcriptional regulatory networks in *Saccharomyces cerevisiae*. *Science* **298**, 799-804. doi:10.1126/science.1075090

Levitan, D. and Greenwald, I. (1998). LIN-12 protein expression and localization during vulval development in *C. elegans*. *Development* **125**, 3101-3109.

Lukoseviciute, M., Gavriouchkina, D., Williams, R. M., Hochgreb-Hagele, T., Senanayake, U., Chong-Morrison, V., Thongjuea, S., Repapi, E., Mead, A. and Sauka-Spengler, T. (2018). From pioneer to repressor: bimodal foxd3 activity dynamically remodels neural crest regulatory landscape in vivo. *Dev. Cell* **47**, 608-628.e6. doi:10.1016/j.devcel.2018.11.009

Luscombe, N. M., Babu, M. M., Yu, H., Snyder, M., Teichmann, S. A. and Gerstein, M. (2004). Genomic analysis of regulatory network dynamics reveals large topological changes. *Nature* **431**, 308-312. doi:10.1038/nature02782

Ma, Y., Kanakousaki, K. and Buttitta, L. (2015). How the cell cycle impacts chromatin architecture and influences cell fate. *Front. Genet.* **5**, 1-18. doi:10.3389/fgene.2015.00019

Maduro, M. F. (2009). Structure and evolution of the *C. elegans* embryonic endomesoderm network. *Biochim. Biophys. Acta Gene Regul. Mech.* **1789**, 250-260. doi:10.1016/j.bbagrm.2008.07.013

Mangan, S. and Alon, U. (2003). Structure and function of the feed-forward loop network motif. *Proc. Natl. Acad. Sci. USA* **100**, 11980-11985. doi:10.1073/pnas.2133841100

Martik, M. L. and McClay, D. R. (2015). Deployment of a retinal determination gene network drives directed cell migration in the sea urchin embryo. *eLife* **4**, e08827. doi:10.7554/eLife.08827

Martinez, M. A. Q., Kinney, B. A., Medwig-Kinney, T. N., Ashley, G., Ragle, J. M., Johnson, L., Aguilera, J., Hammell, C. M., Ward, J. D. and Matus, D. Q. (2019). Rapid degradation of *Caenorhabditis elegans* proteins at single-cell resolution with a synthetic auxin. *G3 (Bethesda)* **9**, g3.400781.2019. doi:10.1534/g3.119.400781

Matus, D. Q., Li, X.-Y., Durbin, S., Agarwal, D., Chi, Q., Weiss, S. J. and Sherwood, D. R. (2010). In vivo identification of regulators of cell invasion across basement membranes. *Sci. Signal.* **3**, ra35. doi:10.1126/scisignal.2000654

Matus, D. Q., Chang, E., Makohon-Moore, S. C., Hagedorn, M. A., Chi, Q. and Sherwood, D. R. (2014). Cell division and targeted cell cycle arrest opens and stabilizes basement membrane gaps. *Nat. Commun.* **5**, 4184. doi:10.1038/ncomms5184

Matus, D. Q., Lohmer, L. L., Kelley, L. C., Schindler, A. J., Kohrman, A. Q., Barkoulas, M., Zhang, W., Chi, Q. and Sherwood, D. R. (2015). Invasive cell fate requires G1 cell-cycle arrest and histone deacetylase-mediated changes in gene expression. *Dev. Cell* **35**, 162-174. doi:10.1016/j.devcel.2015.10.002

Medwig, T. N. and Matus, D. Q. (2017). Breaking down barriers: the evolution of cell invasion. *Curr. Opin. Genet. Dev.* **47**, 33-40. doi:10.1016/j.gde.2017.08.003

Milo, R., Shen-Orr, S., Itzkovitz, S., Kashtan, N., Chklovskii, D. and Alon, U. (2002). Network motifs: simple building blocks of complex networks. *Science* **298**, 824-827. doi:10.1126/science.298.5594.824

Morrissey, M. A., Keeley, D. P., Hagedorn, E. J., McClatchey, S. T. H., Chi, Q., Hall, D. H. and Sherwood, D. R. (2014). B-LINK: a Hemicentin, Plakin, and integrin-dependent adhesion system that links tissues by connecting adjacent basement membranes. *Dev. Cell* **31**, 319-331. doi:10.1016/j.devcel.2014.08.024

Penn, B. H., Bergstrom, D. A., Dilworth, F. J., Bengal, E. and Tapscott, S. J. (2004). A MyoD-generated feed-forward circuit temporally patterns gene expression during skeletal muscle differentiation. *Genes Dev.* **18**, 2348-2353. doi:10.1101/gad.1234304

Porta-de-la-Riva, M., Fontrodona, L., Villanueva, A. and Cerón, J. (2012). Basic *Caenorhabditis elegans* methods: synchronization and observation. *J. Vis. Exp.* **64**, e4019. doi:10.3791/4019

Red-Horse, K., Zhou, Y., Genbacev, O., Prakobphol, A., Foulk, R., McMaster, M. and Fisher, S. J. (2004). Trophoblast differentiation during embryo implantation and formation of the maternal-fetal interface. *J. Clin. Invest.* **114**, 744-754. doi:10.1172/JCI200422991

Reece-Hoyes, J. S., Pons, C., Diallo, A., Mori, A., Shrestha, S., Kadreppa, S., Nelson, J., DiPrima, S., Dricot, A., Lajoie, B. R. et al. (2013). Extensive rewiring and complex evolutionary dynamics in a *C. elegans* multiparameter transcription factor network. *Mol. Cell* **51**, 116-127. doi:10.1016/j.molcel.2013.05.018

Rimann, I. and Hajnal, A. (2007). Regulation of anchor cell invasion and uterine cell fates by the egl-43 Evi-1 proto-oncogene in *Caenorhabditis elegans*. *Dev. Biol.* **308**, 187-195. doi:10.1016/j.ydbio.2007.05.023

Rowe, R. G. and Weiss, S. J. (2008). Breaching the basement membrane: who, when and how? *Trends Cell Biol.* **18**, 560-574. doi:10.1016/j.tcb.2008.08.007

Sallee, M. D., Littleford, H. E. and Greenwald, I. (2017). A bHLH code for sexually dimorphic form and function of the *C. elegans* somatic gonad. *Curr. Biol.* **27**, 1853-1860.e5. doi:10.1016/j.cub.2017.05.059

Saunders, L. R. and McClay, D. R. (2014). Sub-circuits of a gene regulatory network control a developmental epithelial-mesenchymal transition. *Development* **141**, 1503-1513. doi:10.1242/dev.101436

Schindelin, J., Arganda-Carreras, I., Frise, E., Kaynig, V., Longair, M., Pietzsch, T., Preibisch, S., Rueden, C., Saalfeld, S., Schmid, B. et al. (2012). Fiji: an open-source platform for biological-image analysis. *Nat. Methods* **9**, 676-682. doi:10.1038/nmeth.2019

Schindler, A. J. and Sherwood, D. R. (2011). The transcription factor HLH-2/E/Daughterless regulates anchor cell invasion across basement membrane in C. elegans. *Dev. Biol.* **357**, 380-391. doi:10.1016/j.ydbio.2011.07.012

Shen-Orr, S. S., Milo, R., Mangan, S. and Alon, U. (2002). Network motifs in the transcriptional regulation network of Escherichia coli. *Nat. Genet.* **31**, 64-68. doi:10.1038/ng881

Sherwood, D. R. and Plastino, J. (2018). Invading, leading and navigating cells in *Caenorhabditis elegans*: Insights into cell movement in vivo. *Genetics* **208**, 53-78. doi:10.1534/genetics.117.300082

Sherwood, D. R. and Sternberg, P. W. (2003). Anchor cell invasion into the vulval epithelium in *C. elegans*. *Dev. Cell* **5**, 21-31. doi:10.1016/S1534-5807(03)00168-0

Sherwood, D. R., Butler, J. A., Kramer, J. M. and Sternberg, P. W. (2005). FOS-1 promotes basement-membrane removal during anchor-cell invasion in *C. elegans*. *Cell* **121**, 951-962. doi:10.1016/j.cell.2005.03.031

Simmer, F., Tijsterman, M., Parrish, S., Koushika, S. P., Nonet, M. L., Fire, A., Ahringer, J., Plasterk, R. H. A., Louis, S., Road, T. C. et al. (2002). Loss of the putative RNA-directed RNA polymerase RRF-3 makes *C. elegans* hypersensitive to RNAi. *Current* **12**, 1317-1319. doi:10.1016/S0960-9822(02)01041-2

Skene, P. J. and Henikoff, S. (2017). An efficient targeted nuclease strategy for high-resolution mapping of DNA binding sites. *eLife* **6**, e21856. doi:10.7554/eLife.21856

Sturm, Á., Saskői, É., Tibor, K., Weinhardt, N. and Vellai, T. (2018). Highly efficient RNAi and Cas9-based auto-cloning systems for *C. elegans* research. *Nucleic Acids Res.* **46**, e105. doi:10.1093/nar/gky516

Swift, J. and Coruzzi, G. M. (2017). A matter of time – how transient transcription factor interactions create dynamic gene regulatory networks. *Biochim. Biophys. Acta Gene Regul. Mech.* **1860**, 75-83. doi:10.1016/j.bbagrm.2016.08.007

Vega, S., Morales, A. V., Ocaña, O. H., Valdés, F., Fabregat, I. and Nieto, M. A. (2004). Snail blocks the cell cycle and confers resistance to cell death. *Genes Dev.* **18**, 1131-1143. doi:10.1101/gad.294104

Verghese, E., Schocken, J., Jacob, S., Wimer, A. M., Royce, R., Nesmith, J. E., Baer, G. M., Clever, S., McCain, E., Lakowski, B. et al. (2011). The tailless ortholog nhr-67 functions in the development of the *C. elegans* ventral uterus. *Dev. Biol.* **356**, 516-528. doi:10.1016/j.ydbio.2011.06.007

Wang, L., Shen, W., Lei, S., Matus, D., Sherwood, D. and Wang, Z. (2014). MIG-10 (lamellipodin) stabilizes invading cell adhesion to basement membrane and is a negative transcriptional target of EGL-43 in *C. elegans*. *Biochem. Biophys. Res. Commun.* **452**, 328-333. doi:10.1016/j.bbrc.2014.08.049

Wilkinson, H. A., Fitzgerald, K. and Greenwald, I. (1994). Reciprocal changes in expression of the receptor lin-12 and its ligand lag-2 prior to commitment in a *C. elegans* cell fate decision. *Cell* **79**, 1187-1198. doi:10.1016/0092-8674(94)90010-8

Xie, Q. and Cvekl, A. (2011). The orchestration of mammalian tissue morphogenesis through a series of coherent feed-forward loops. *J. Biol. Chem.* **286**, 43259-43271. doi:10.1074/jbc.M111.264580

Yakoby, N., Lembong, J., Schupbach, T. and Shvartsman, S. Y. (2007). *Drosophila* eggshell is patterned by sequential action of feedforward and feedback loops. *Development* **135**, 343-351. doi:10.1242/dev.008920

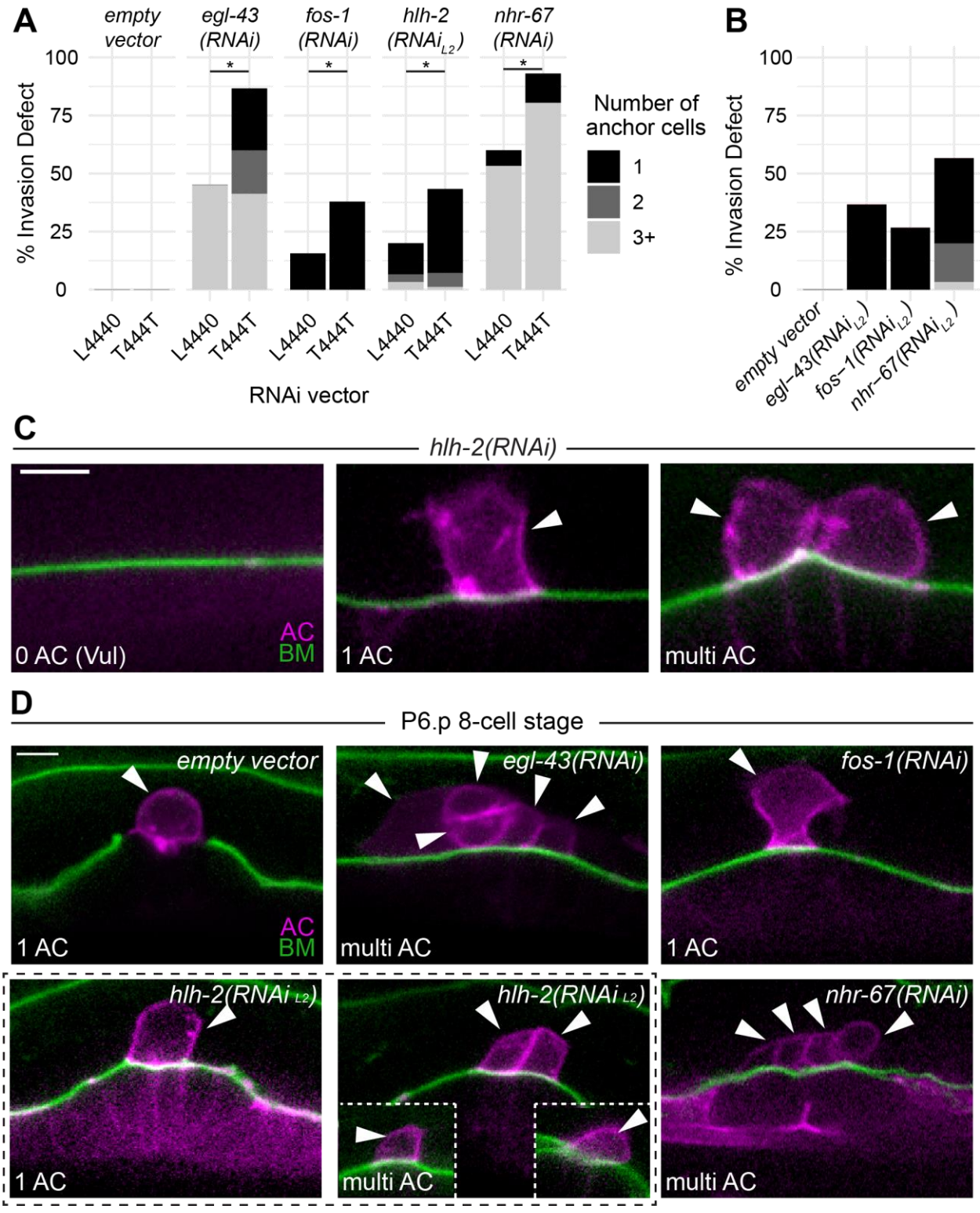

Fig. S1. Improved RNAi vector increases penetrance of TF depletion phenotypes. (A) Stacked bar graph depicting the penetrance of AC invasion defects at the P6.p 4-cell stage comparing L4440-based versus T444T-based RNAi depletions in a uterine-specific RNAi-hypersensitive background. Asterisk (*) denotes a statistically significant difference between the vectors and represents a p-value < 0.03 by Fisher's exact test (n ≧ 30 animals per treatment). (B) Stacked bar graphs depicting AC invasion defects following delayed TF-RNAi treatment at the L2 stage (n = 30 animals per treatment). (C) Single plane of confocal z-stack depicting early depletion of *hlh-2* at the L1 stage. The AC-specific membrane marker (magenta, *cdh-3*$^{1.5}$>mCherry::PLCδ^{PH}) and BM marker (green, *lam-1*>LAM-1::GFP) are overlaid in each micrograph. (D) Single plane of confocal z-stacks during the L4 stage (P6.p 8-cell stage) depicting representative phenotypes associated with TF-RNAi treatment.

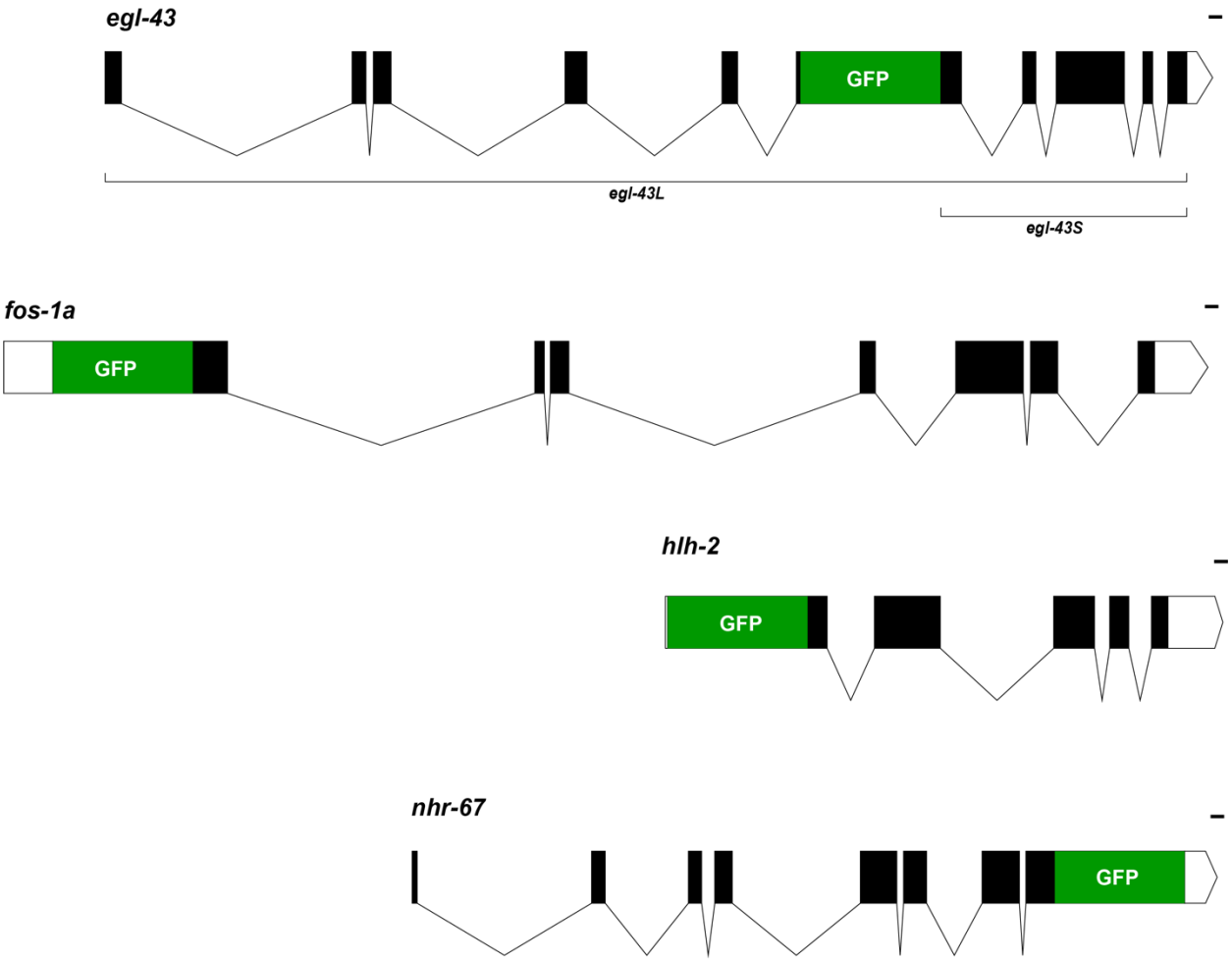

Fig. S2. Schematic of endogenous GFP-tagged loci of pro-invasive TFs. Codon-optimized GFP was integrated at the N-terminus of *fos-1A* and *hlh-2,* at the C-terminus of *nhr-67*, and internally in the *egl-43* locus (tagging both isoforms). This figure was made using http://wormweb.org/exonintron. Scale bar, 100 bp.

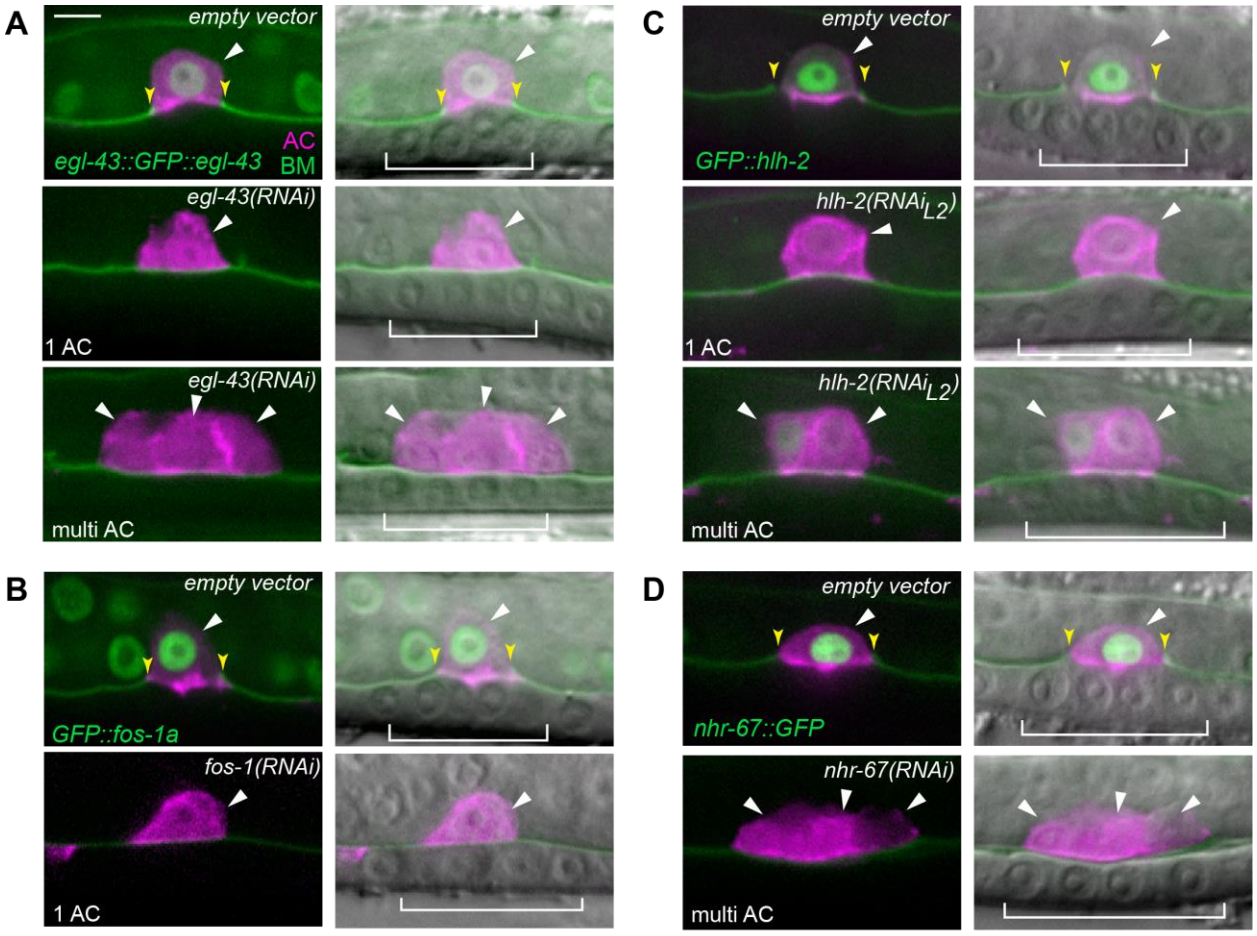
A
empty vector
egl-43::GFP::egl-43
AC
BM
egl-43(RNAi)
1 AC
egl-43(RNAi)
multi AC
B
empty vector
GFP::fos-1a
fos-1(RNAi)
1 AC
C
empty vector
GFP::hlh-2
hlh-2(RNAi L2)
1 AC
hlh-2(RNAi L2)
multi AC
D
empty vector
nhr-67::GFP
nhr-67(RNAi)
multi AC

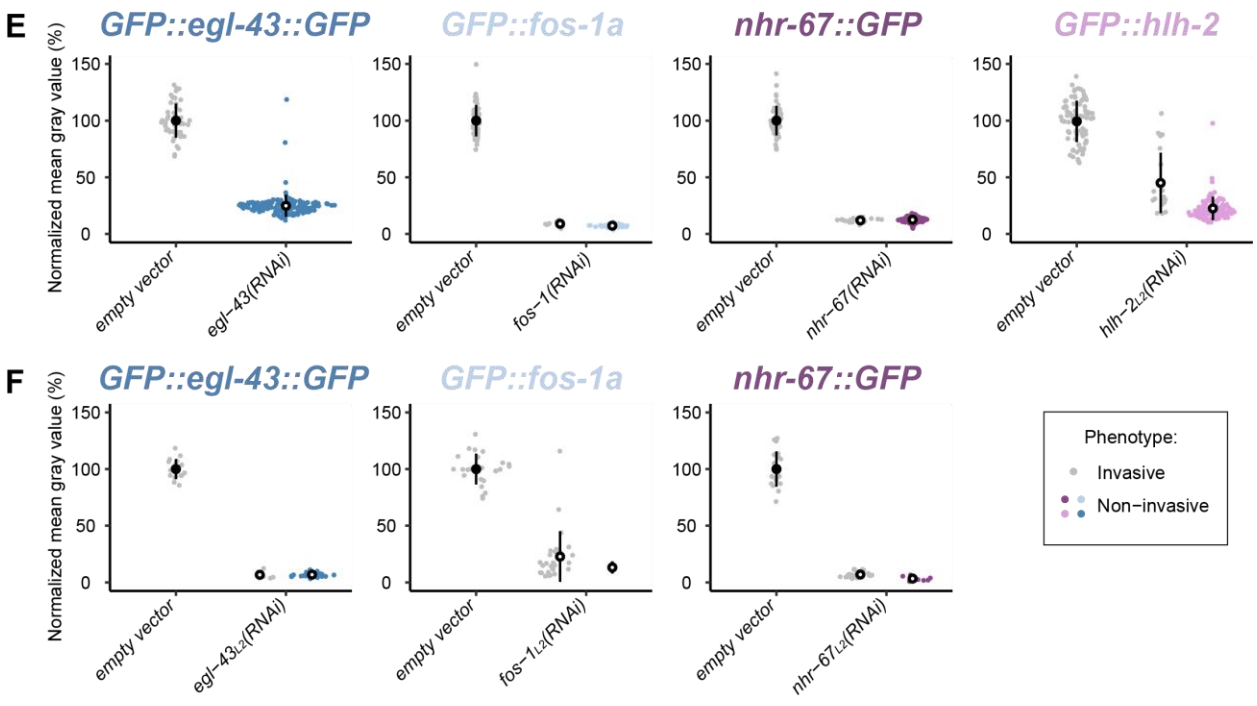
E
GFP::egl-43::GFP
GFP::fos-1a
nhr-67::GFP
GFP::hlh-2
Normalized mean gray value (%)
150
100
50
0
empty vector
egl-43(RNAi)
fos-1(RNAi)
nhr-67(RNAi)
hlh-2L2(RNAi)
F
GFP::egl-43::GFP
GFP::fos-1a
nhr-67::GFP
egl-43L2(RNAi)
fos-1L2(RNAi)
nhr-67L2(RNAi)
Phenotype:
Invasive
Non-invasive

Figure S3. AC invasion phenotypes do not necessarily correlate to TF expression levels. (A-D) Single planes of confocal z-stack depicting representative phenotype (single vs. multi AC, bottom left of each image) of fluorescence alone (left; AC, magenta, expressing *cdh-3*>mCherry::moeABD and BM, green) and DIC overlay (right). (E) Sina plots of GFP-tagged TF levels, defined as the mean gray value of individual AC nuclei at the P6.p 4-cell stage following TF-RNAi knockdown. In this and all other figures, statistical significance as compared to empty vector controls is denoted as an open black circle and here represents a p-value of $< 1\times10^{-6}$ by Student's t test ($n \geq 50$ animals per treatment).

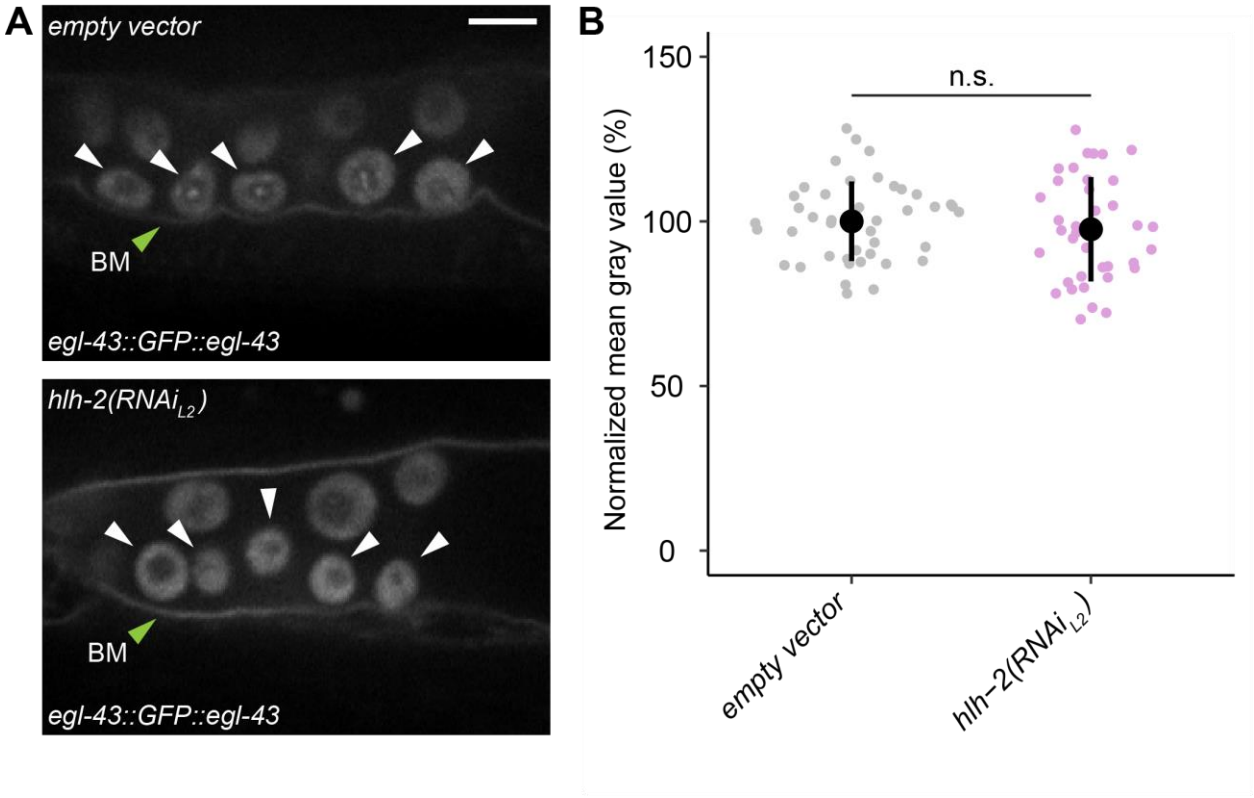

Fig S4. HLH-2 does not regulate EGL-43 expression in the ventral uterus. (A) Single plane of confocal z-stack depicting levels of *egl-43::GFP::egl-43* in the ventral uterine (VU) cells (white arrowheads) in empty vector controls (top) as compared to *hlh-2(RNAi)* depletion. BM indicated by green arrowheads. (B) Sina plots of *egl-43::GFP::egl-43* levels, defined as the mean gray value of individual VU nuclei, following *hlh-2* RNAi treatment (n ≥ 10 animals, n ≧ 37 VU cells quantified per treatment; n.s., not significant, p-value = 0.45, Student's t-test).

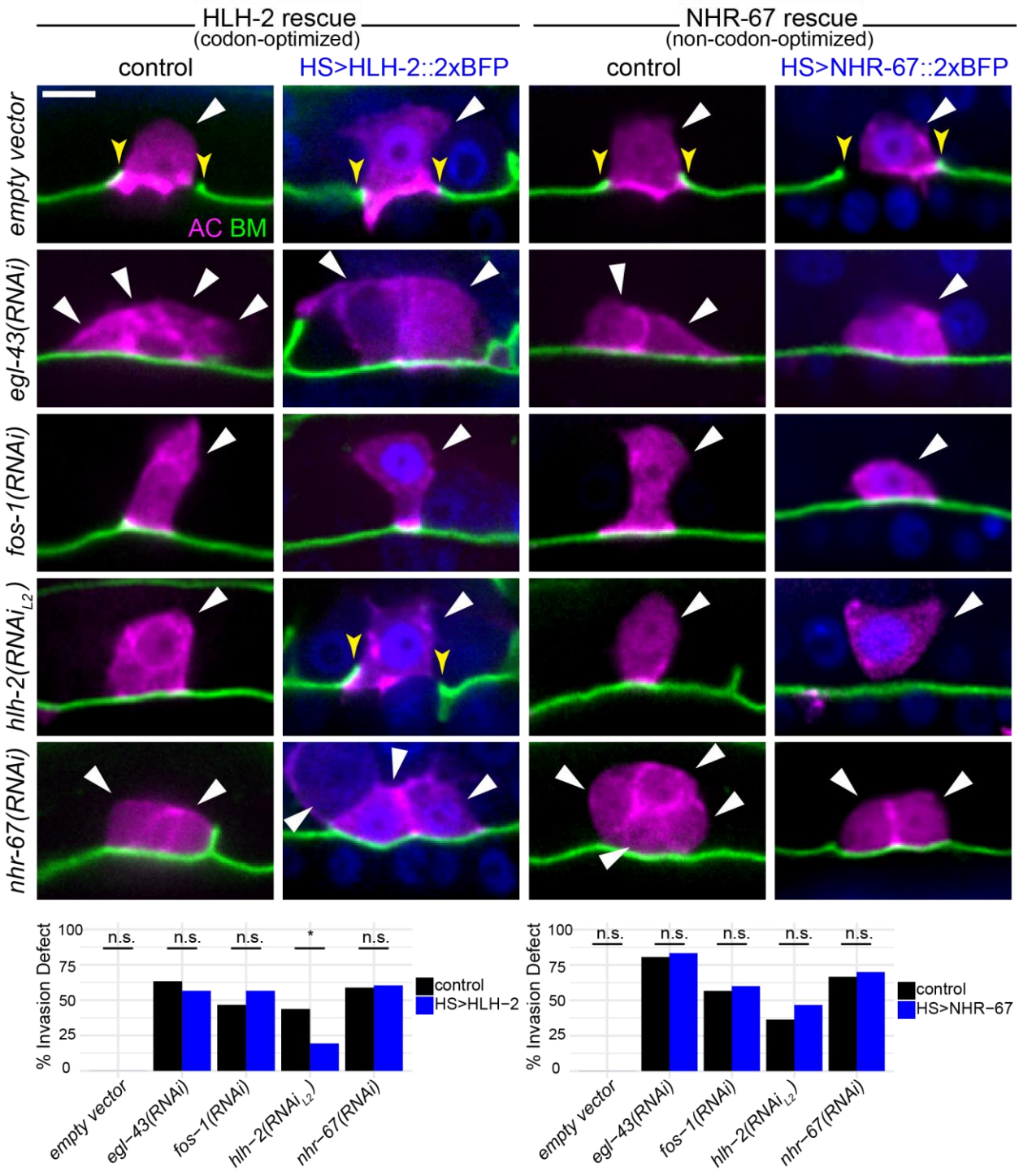

Figure S5. Induced expression of *hlh-2* and *nhr-67* reveal cell cycle independent roles for *hlh-2*. (A-B) Single planes of confocal z-stack depicting representative phenotype (single vs. multi AC) as fluorescence overlays (AC, magenta, expressing *cdh-3*>mCherry::moeABD, and BM, green) following no heat shock control (left) as compared

to heat shock induced expression of HLH-2::2xTagBFP (blue) (A) and NHR-67::2xTagBFP (B). (C-D) Bar graphs depict the penetrance of invasion defects in control (black) compared to heat shock induced HLH-2 (C) and NHR-67 (D) at the P6.p 4-cell stage (n ≥ 30 animals examined for each RNAi treatment; n.s., not significant; *p-value < 1×10^{-6}; Fisher's exact test).

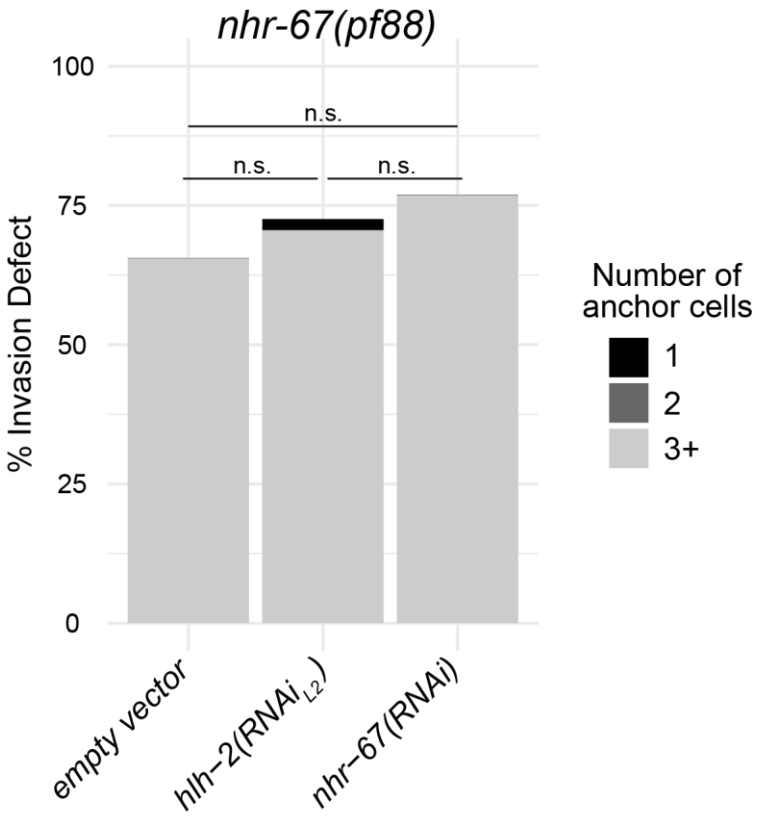

Figure S6. Depletion of *hlh-2* does not significantly increase the invasion defect of an *nhr-67(pf88)* hypomorph. Bar graph depicts the penetrance of AC invasion defects at the P6.p 4-cell stage in control (empty vector) as compared to *hlh-2(RNAi$_{L2}$)* or *nhr-67(RNAi)* treatment (n ≧ 50 animals examined for each RNAi treatment, n.s. not significant, Fisher's exact, p-value = 0.5350 (empty vector vs. *hlh-2*), 0.1690 (empty vector vs. *nhr-67*) and 0.6676 (*hlh-2* vs. *nhr-67*)).

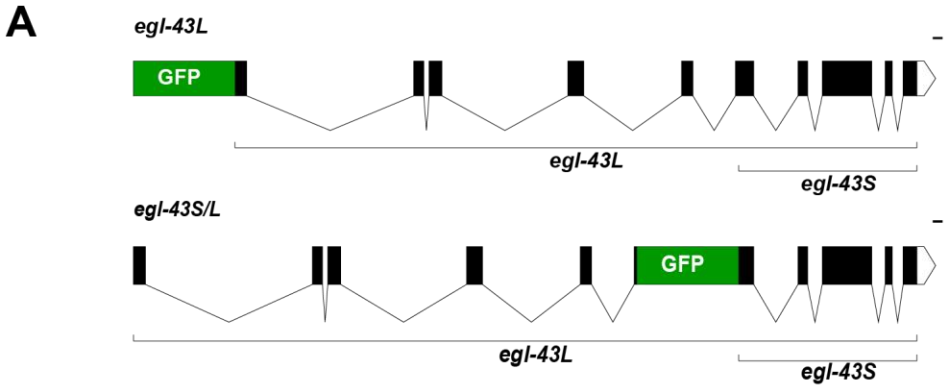

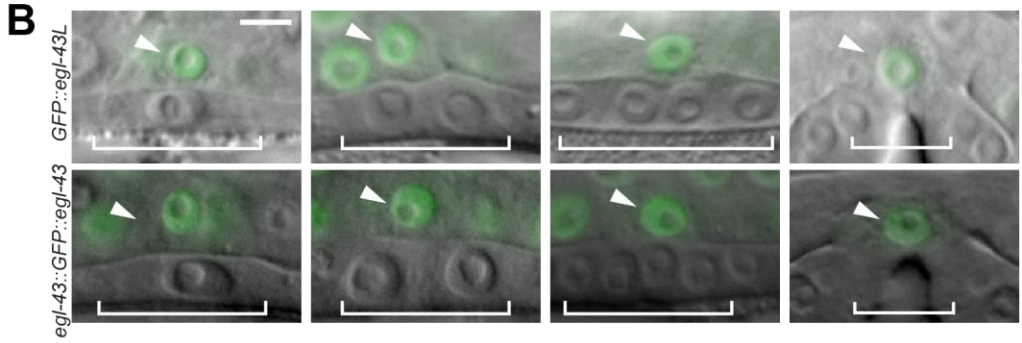

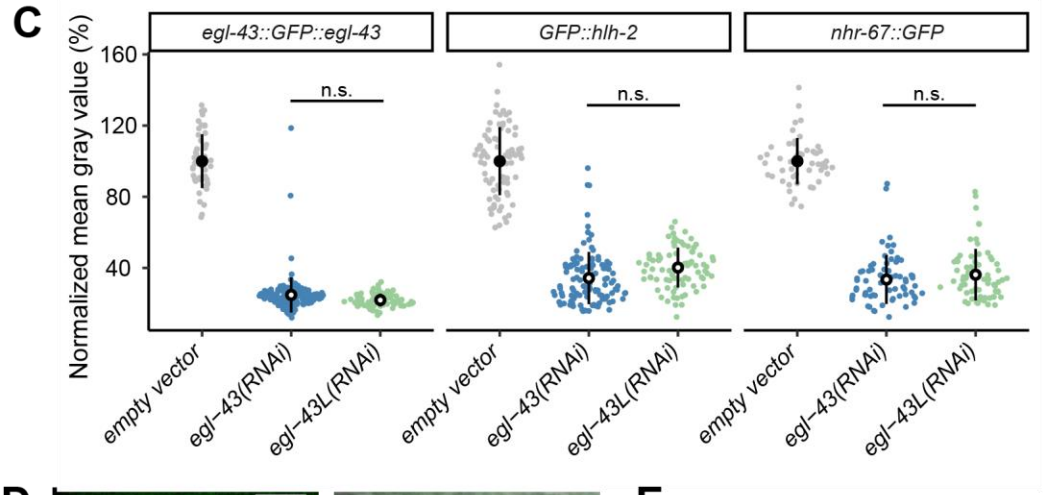

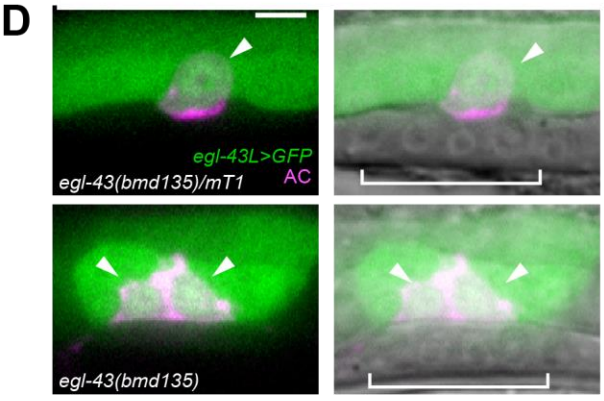

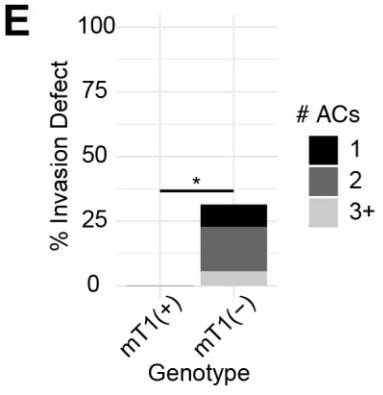

Figure S7. Both isoforms of *egl-43* function redundantly to regulate AC invasion. (A) Schematics (via http://wormweb.org/exonintron) of GFP insertion into the *egl-43* locus to tag the long (top) or both isoforms (bottom). Scale bar, 100 bp. (B) DIC overlaid with single confocal planes of *GFP::egl-43L* (top) and *egl-43::GFP::egl-43* (bottom). (C) Sina plots of GFP-tagged TF levels, defined as the mean gray value of individual AC nuclei, following RNAi perturbation ($n \geq 25$ animals for each treatment; n.s., not significant) between RNAi treatments targeting *egl-43L* and *egl-43*. (D) Single plane of confocal z-stacks depicting representative micrographs of control (top) versus *egl-43(bmd135)* animals expressing *egl-43L>GFP* (green) and an AC reporter (magenta). (E) Stacked bar graph depicting penetrance of AC invasion defect. Asterisk (*) denotes statistical significance between control and mT1(-) animals and represents a p-value $< 1\times10^{-3}$ by Fisher's exact test ($n \geq 25$ animals per treatment).

Table S1: Scoring table

**percentages may not necessarily sum to 100 due to rounding*

Genotype	RNAi Treatment (gene, vector, L1/L2 plating)			P6.p stage	% Invaded (#ACs)				% Not invaded (#ACs)				n
					0	1	2	3+	0	1	2	3+	
rrf-3(pk1426) II; unc-119(ed3) III; rde-1(ne219) V; fos-1a>RDE-1, myo-2>YFP; cdh-3>PH::mCherry; lam-1>LAM-1::GFP + unc-119(+)	*empty vector*	T444T	L1	4-cell	0	100	0	0	0	0	0	0	50
	egl-43(RNAi)	T444T	L1	4-cell	0	12	1	0	0	27	19	41	75
	egl-43(RNAi)	T444T	L2	4-cell	0	63	0	0	0	37	0	0	30
	egl-43L(RNAi)	T444T	L1	4-cell	0	41	1	0	0	19	15	24	80
	fos-1(RNAi)	T444T	L1	4-cell	0	62	0	0	0	38	0	0	66
	fos-1(RNAi)	T444T	L2	4-cell	0	73	0	0	0	27	0	0	30
	hlh-2(RNAi)	T444T	L1	4-cell	0	30	0	0	21	37	6	5	115
	hlh-2(RNAi)	T444T	L2	4-cell	0	57	0	0	0	36	6	1	83
	nhr-67(RNAi)	T444T	L1	4-cell	0	7	0	0	0	13	0	81	72
	nhr-67(RNAi)	T444T	L2	4-cell	0	43	0	0	0	37	17	3	30
	empty vector	T444T	L1	8-cell	0	100	0	0	0	0	0	0	50
	egl-43(RNAi)	T444T	L1	8-cell	0	40	5	5	0	0	4	45	55
	egl-43L(RNAi)	T444T	L1	8-cell	0	78	9	5	0	7	0	2	58
	fos-1(RNAi)	T444T	L1	8-cell	0	90	0	0	0	10	0	0	50
	hlh-2(RNAi)	T444T	L1	8-cell	0	41	3	0	24	24	1	8	76
	hlh-2(RNAi)	T444T	L2	8-cell	0	64	1	1	0	23	1	9	81
	nhr-67(RNAi)	T444T	L1	8-cell	0	32	0	0	0	0	0	68	57
	empty vector	L4440	L1	4-cell	0	100	0	0	0	0	0	0	30
	egl-43(RNAi)	L4440	L1	4-cell	0	55	0	0	0	0	0	45	31
	fos-1(RNAi)	L4440	L1	4-cell	0	84	0	0	0	16	0	0	32
	hlh-2(RNAi)	L4440	L1	4-cell	0	69	0	0	9	16	0	6	32
	hlh-2(RNAi)	L4440	L2	4-cell	0	80	0	0	0	13	3	3	30
	nhr-67(RNAi)	L4440	L1	4-cell	0	40	0	0	0	7	0	53	30
cdh-3(5kb)>CKI-1::GFP; zmp-1>mCherry	*empty vector*	T444T	L1	4-cell	0	100	0	0	0	0	0	0	51
	egl-43(RNAi)	T444T	L1	4-cell	0	10	0	0	0	90	0	0	31
	fos-1(RNAi)	T444T	L1	4-cell	0	20	0	0	0	80	0	0	35
	hlh-2(RNAi)	T444T	L2	4-cell	0	92	0	0	0	8	0	0	77
	nhr-67(RNAi)	T444T	L1	4-cell	0	100	0	0	0	0	0	0	42
laminin::GFP; zmp-1>mCherry	*empty vector*	T444T	L1	4-cell	0	100	0	0	0	0	0	0	27
	egl-43(RNAi)	T444T	L1	4-cell	0	19	3	0	0	30	22	27	37
	fos-1(RNAi)	T444T	L1	4-cell	0	49	0	0	0	51	0	0	53
	hlh-2(RNAi)	T444T	L2	4-cell	0	56	0	0	0	31	3	10	59
	nhr-67(RNAi)	T444T	L1	4-cell	0	47	0	0	0	0	35	18	62
egl-43>LoxP::GFP::EGL-43; cdh-3>mCherry::moeABD; laminin::GFP	*empty vector*	T444T	L1	4-cell	0	100	0	0	0	0	0	0	68
	egl-43(RNAi)	T444T	L1	4-cell	0	0	0	0	0	8	14	78	158
	egl-43(RNAi)	T444T	L2	4-cell	0	16	0	0	0	78	0	6	32
hlh-2>LoxP::GFP::HLH-2; cdh-3>mCherry::moeABD; laminin::GFP	*empty vector*	T444T	L1	4-cell	0	100	0	0	0	0	0	0	83
	hlh-2(RNAi)	T444T	L2	4-cell	0	24	0	0	0	76	0	0	50
fos-1>LoxP::GFP::FOS-1; cdh-3>mCherry::moeABD; laminin::GFP	*empty vector*	T444T	L1	4-cell	0	100	0	0	0	0	0	0	74
	fos-1(RNAi)	T444T	L1	4-cell	0	18	0	0	0	9	5	68	120
	fos-1(RNAi)	T444T	L2	4-cell	0	93	0	0	0	7	0	0	30
nhr-67>NHR-67::GFP; cdh-3>mCherry::moeABD; laminin::GFP	*empty vector*	T444T	L1	4-cell	0	100	0	0	0	0	0	0	70
	nhr-67(RNAi)	T444T	L1	4-cell	0	15	1	0	0	0	11	73	130
	nhr-67(RNAi)	T444T	L2	4-cell	0	76	0	0	0	6	0	18	34
egl-43L>SEC::GFP::EGL-43; laminin::GFP; cdh-3>mCherry::moeABD;	*N/A*			4-cell	0	67	3	0	0	8	17	6	51
egl-43L>SEC::GFP::EGL-43/mT1; laminin::GFP; cdh-3>mCherry::moeABD	*N/A*			4-cell	0	100	0	0	0	0	0	0	25
nhr-67(pf88); qyIs227[cdh-3>mCherry::moeABD] I; qyIs7[laminin::GFP] X.	*empty vector*	T444T	L1	4-cell	0	34	0	0	0	0	0	66	58
	hlh-2(RNAi)	T444T	L1	4-cell	0	23	0	0	0	0	0	77	51
	nhr-67(RNAi)	T444T	L1	4-cell	0	27	0	0	0	1	0	71	65

Table S2: Rescue experiments

**percentages may not necessarily sum to 100 due to rounding*

Genotype	Condition	RNAi Treatment (gene, vector, L1/L2 plating)			P6.p stage	% Invaded	% Not Invaded	n
bmd142[hsp>HLH-2::2xBFP] I; qyIs225[cdh-3>mCherry::moeABD] V; qyIs7[laminin::GFP] X.	control	*empty vector*	T444T	L1	4-cell	100	0	30
	control	*egl-43(RNAi)*	T444T	L1	4-cell	37	63	30
	control	*fos-1(RNAi)*	T444T	L1	4-cell	53	47	30
	control	*hlh-2(RNAi)*	T444T	L2	4-cell	56	44	32
	control	*nhr-67(RNAi)*	T444T	L1	4-cell	41	59	34
	heat shocked	*empty vector*	T444T	L1	4-cell	100	0	30
	heat shocked	*egl-43(RNAi)*	T444T	L1	4-cell	43	57	30
	heat shocked	*fos-1(RNAi)*	T444T	L1	4-cell	43	57	30
	heat shocked	*hlh-2(RNAi)*	T444T	L2	4-cell	81	19	31
	heat shocked	*nhr-67(RNAi)*	T444T	L1	4-cell	40	60	43
bmd121[LoxP::hsp>NHR-67::2xBFP] I; qyIs227[cdh-3>mCherry::moeABD] I; qyIs7[laminin::GFP] X.	control	*empty vector*	T444T	L1	4-cell	100	0	30
	control	*egl-43(RNAi)*	T444T	L1	4-cell	19	81	30
	control	*fos-1(RNAi)*	T444T	L1	4-cell	43	57	31
	control	*hlh-2(RNAi)*	T444T	L2	4-cell	64	36	33
	control	*nhr-67(RNAi)*	T444T	L1	4-cell	33	67	30
	heat shocked	*empty vector*	T444T	L1	4-cell	100	0	30
	heat shocked	*egl-43(RNAi)*	T444T	L1	4-cell	17	83	30
	heat shocked	*fos-1(RNAi)*	T444T	L1	4-cell	40	60	30
	heat shocked	*hlh-2(RNAi)*	T444T	L2	4-cell	53	47	30
	heat shocked	*nhr-67(RNAi)*	T444T	L1	4-cell	30	70	30

Table S3: Strains

Strain	Genotype	Description	Figure(s)	Source
NK1316	*rrf-3(pk1426) II; unc-119(ed3) III; rde-1(ne219) V; qyIs102[fos-1a>RDE-1, myo-2>YFP]; qyIs24[cdh-3>PH::mCherry]; qyIs10[lam-1>LAM-1::GFP with unc-119(with)]*	uterine-specific RNAi strain with AC and BM markers	1, 6, S1	Matus et al., 2015
GS9129	*arTi145[ckb-3>mCherry::H2B] II; lin-12(ar624[lin-12>LIN-12::GFP]) III.*	endogenous *lin-12* GFP reporter with somatic gonad marker	2, 7	Attner et al., 2019
DQM337	*egl-43(bmd88[egl-43>LoxP::GFP::EGL-43]) II; qyIs225[cdh-3>mCherry::moeABD] V.*	endogenous *egl-43* GFP reporter with AC marker	2, S7	This study
DQM497	*fos-1(bmd138[fos-1>LoxP::GFP::FOS-1]) V.*	endogenous *fos-1* GFP reporter	2	This study
DQM352	*hlh-2(bmd90[hlh-2>LoxP::GFP::HLH-2]) I; qyIs225[cdh-3>mCherry::moeABD] V.*	endogenous *hlh-2* GFP reporter with AC marker	2	This study
DQM291	*nhr-67(syb509[nhr-67>NHR-67::GFP]) IV; qyIs227[cdh-3>mCherry::moeABD] I.*	endogenous *nhr-67* GFP reporter with AC marker	2	This study
DQM335	*egl-43(bmd88[egl-43>LoxP::GFP::EGL-43]) II; qyIs225[cdh-3>mCherry::moeABD] V; qyIs7[laminin::GFP] X.*	endogenous *egl-43* GFP reporter with AC and BM markers	2-3, 7, S3, S4, S7	This study
DQM515	*fos-1(bmd138[fos-1>LoxP::GFP::FOS-1]) V; qyIs227[cdh-3>mCherry::moeABD] I; qyIs7[laminin::GFP] X.*	endogenous *fos-1* GFP reporter with AC and BM markers	2-3, 7, S3	This study
DQM350	*hlh-2(bmd90[hlh-2>LoxP::GFP::HLH-2]) I; qyIs225[cdh-3>mCherry::moeABD] V; qyIs7[laminin::GFP] X.*	endogenous *hlh-2* GFP reporter with AC and BM markers	2-3, 7, S3, S7	This study
DQM368	*nhr-67(syb509[nhr-67>NHR-67::GFP]) IV; qyIs225[cdh-3>mCherry::moeABD] V; qyIs7[laminin::GFP] X.*	endogenous *nhr-67* GFP reporter with AC and BM markers	2-3, 7, S3, S7	This study
DQM7	*qyIs330 [laminin::mCherry]; qyIs232 [CDT-1::GFP]*	G1 cell cycle phase reporter with BM marker	4	Matus et al., 2015
DQM533	*zmp-1(qy17[zmp-1::LoxP::GFP]) III; qyIs225[cdh-3>mCherry::moeABD] V*	endogenous *zmp-1* GFP reporter with AC marker	4	This study
DQM39	*qyIs17 [zmp-1>mCherry] II; qyIs266[cdh-3(5kb)>CKI-1::GFP] V*	*zmp-1* mCherry reporter with AC-specific CKI-1 over-expression	5	Matus et al., 2015
NK272	*qyIs7[laminin::GFP]; qyIs17[zmp-1>mCherry]*	*zmp-1* mCherry reporter with BM marker	5	Matus et al., 2015
DQM503	*egl-43(bmd87[egl-43>SEC::GFP::EGL-43] II/mT1; qyIs227[cdh-3>mCherry::moeABD] I; qyIs7[laminin::GFP] X.*	endogenous *egl-43* transcriptional reporter (with SEC) balanced over mT1 with AC and BM markers	6	This study
DQM444	*bmd121[LoxP::hsp>NHR-67::2xBFP] I; qyIs227[cdh-3>mCherry::moeABD] I; qyIs7[laminin::GFP] X.*	heat shock inducible NHR-67 with AC and BM markers	S5	This study
DQM552	*bmd142[hsp>HLH-2::2xBFP] I; qyIs225[cdh-3>mCherry::moeABD] V; qyIs7[laminin::GFP] X.*	heat shock inducible HLH-2 (codon-optimized) with AC and BM markers	S5	This study
DQM266	*nhr-67(pf88); qyIs227[cdh-3>mCherry:: moeABD] I; qyIs7[laminin::GFP] X.*	nhr-67 hypomorphic mutant with AC and BM markers	S6	This study
DQM500	*bmd135[egl-43L>SEC::GFP::EGL-43] II/mT1; qyIs227[cdh-3>mCherry::moeABD] I; qyIs7[laminin::GFP] X.*	endogenous *egl-43L* transcriptional reporter (with SEC) balanced with mT1 balancer with AC and BM markers	S7	This study
DQM494	*egl-43(bmd136[egl-43L>LoxP::GFP::EGL-43]) II.*	endogenous *egl-43L* GFP reporter	S7	This study
DQM300	*egl-43(bmd88[egl-43>LoxP::GFP::EGL-43]) II.*	endogenous egl-43 GFP reporter	Will be made available through the CGC (cgc.umn.edu)	
DQM497	*fos-1(bmd138[fos-1>LoxP::GFP::FOS-1]) V.*	endogenous fos-1 GFP reporter		
DQM311	*hlh-2(bmd90[hlh-2>LoxP::GFP::HLH-2]) I.*	endogenous hlh-2 GFP reporter		
PHX509	*nhr-67(syb509[nhr-67>NHR-67::GFP]) IV.*	endogenous nhr-67 GFP reporter		

Table S4: Primers

Primer	Primer sequence (5'→3')	Primer type	Amplicon	Template
DQM657	tcactatagggagaccggcaATG	Forward	*hlh-2* and *nhr-67* synthesized DNAs for T444T	Twist Biosciences gene fragments for *hlh-2, nhr-67*
DQM658	attgggtaccgggcccc	Reverse		
DQM688	gagctcAGATCTatgagcatcgacacagacttc	Forward	BglII-*egl-43L*-XhoI for T444T	Twist Biosciences gene fragment for *egl-43L*
DQM689	acgtacCTCGAGctgactttgacacgttgggc	Reverse		
DQM720	TCACTATAGGGAGACCGGCAATG	Forward	BglII-*egl-43*-SalI for T444T	*egl-43* IDT gBlock
DQM722	GCCCCCCCTCGAGGTCGAACTTTTGGCACCGGAAC	Reverse		
DQM708	ggtttcgccacctctgacttg	Forward	colony PCR screening of T444T constructs	T444T-based constructs
DM191	gtaatacgactcactatagggcgaattgg	Reverse		
DQM433	ACGTTGTAAAACGACGGCCAG	Forward	amplify left homology arm (universal)	Twist Biosciences gene fragments
DQM434	CTCCAGTGAACAATTCTTCTCCTTTACTC	Reverse	amplify left homology arm (universal)	
DQM435	GCGTGATTACAAGGATGACGATGAC	Forward	amplify right homology arm (universal)	
DQM436	GAAACAGCTATGACCATGTTATCGATTTCC	Reverse	amplify right homology arm (universal)	
DQM751	tcctattgcgagatgtcttGTCCACTCTCTTATATAGCAGGTTTTAGAGCTAGAAATAGC	Forward	*fos-1a* sgRNA	pDD122
DQM747	tcctattgcgagatgtcttGgatgctcatcctgaaaacttGTTTTAGAGCTAGAAATAGC	Forward	*egl-43L* sgRNA	pDD122
DQM438	tcctattgcgagatgtcttGaagtcagATGCCATCACAAGGTTTTAGAGCTAGAAATAGC	Forward	*egl-43* sgRNA	pDD122
DQM440	tcctattgcgagatgtcttGAGTTTTCAGAACCTCAATGGGTTTTAGAGCTAGAAATAGC	Forward	*hlh-2* sgRNA	pDD122
DQM412	AGATTGTACTGAGAGTGCACCATATGCGGTGTGAAATACCGCAC	Reverse	amplify sgRNA (universal)	pDD122

Table S5: Plasmids

Plasmid	Base vector	Description
pTNM011	pDD122	*egl-43* internal sgRNA
pTNM012	pDD282	*egl-43::GFP::egl-43* repair template
pTNM013	pDD122	*fos-1* N-terminal sgRNA
pTNM014	pDD282	*GFP::fos-1* repair template
pTNM015	pDD122	*hlh-2* N-terminal sgRNA
pTNM016	pDD282	*GFP::hlh-2* repair template
pTNM046	pDD122	*egl-43L* N-terminal sgRNA
pTNM047	pDD282	*GFP::egl-43L* repair template
pTNM051	pAP088	heat shock inducible HLH-2 (codon-optimized)
pWZ172	T444T	*egl-43* RNAi
pWZ173	T444T	*egl-43L* RNAi
pWZ174	T444T	*fos-1* RNAi
pWZ175	T444T	*hlh-2* RNAi
pWZ176	T444T	*nhr-67* RNAi
pWZ193	pAP088	heat shock inducible NHR-67

Table S6: CRISPR reagents

Gene	Guide	Left homology arm sequence	Right homology arm sequence
egl-43 (internal)	aagtcagatgccatcacaag	CTAAGATATGAGAACCCGTTTACAGAGTCCTTTTA TAGAATTTTGGTTTTTATAATAGAGATGTATGGAA ACCGGGCAAAGTTAATTAGGATTCTTACAGCCAA CAAGAAAATTTTAAGATAAGTAACGACCAAAACTT GAGCGGAGTTGAAAGTTCAGTGCATTACAATTGA AGTTTTTATTTATTATTTATTTATCTTGGGCTAGAA TAGATGGAGCATCTTCACAGGACTGGACTTATAT AATGGCTATCTGCCTGCCTGCCTACCTGCCTTTC GTTTTATTTATACTGTATTTGCGCAATATAAACTCA TGCATTTCTATTTGTTAGAAGTTAAAAAAAACAAT ATTTAGAAAACGTTCACATGTACTTTGATAGTTGG CTCGCATGTTGGCAGAAGGCAGGCACAGGGAAC CCTGAAGGCACTTAGGCAGGTTCGCTGGACAAA ATACCTGCTGATTGTGCTGATTTATTTTCACTAAT ATAATCAGATATGAAACATGGACAATTGGGTACA ATACTAATAGAGGGTGTACTGCTATATAACTTCTC CGAATCAAAACTTAACAGTCATTCACATTCACTAT CACGTGTTATCAATCAATTTTTTTCAGCGGTCTCA AACAACACTCTCATATTCATTGCTCCTTAAAGCCG TTTCGGTGTCATTTGTGTCCAAAGTCCTACACACA ATTCTCAAATCTGTGCAGGCACCGGAGAGTTCAT TCAGTGAGTTATTAATTTAGAGTTTCTAAGAATAA ACTGAGCACTGTAATAATCTATCGTGCAATGCTC CTGGGCTAAGAGTCCTTAAAGAGAGGATATAAAA CTGAATAAACCCCATAATCTCACAACAGGGGGGA AAACTCGAGGCGTGGTCAAGAAGGTTATTGTCCT CTGTACTAATAAAAACGGAAACGATTTCAATGATG TGCCCCCACCTGAGGTGGTCCCTTCCTTAATTGT TTACCCCGTGAGAAAAGTGCAAGGAGCCATGATG CTCCGCCCTCTTTCTTCTCAACCAATAAGACACG CGCGCCGCCCATCCCTCGTGCATCTTCCCTTTGG GGTGTGTCACAGGGCTCATTCTTGTGACGTGCG CTTCCCACCTTTACCAGTGTGTTATCAATCTCCGT CTTATTCATTAGTGAATAAATATTCCAGGACGGTT GGACGTGCCCAACGTGTCAAAGTCAG	ATGCCATCACAAGCGGCACTAACGAAGCATCGAC CAGTTTGCGAGATGACTGCACTCTACAAACCATTG ATGGCGCAACTTGCCGGATTGAGCGGAGCAGGTG GATTAGGTTCCGTGCCATATTGGCCACATATACTT CAAATGGCAACACAGGTTAGTTATTATTTTGAAAAC TCAACTATAGATACCGTCTCCCCTATTACTATTGCA TCCCATTATTCAACTTTGACGCTTTATATTTCAGTT TCCGTTTGTCCTACATGAAAATGATCAATTGGCCA ATTTTTTATTATTTCTTTCTCTATAGTTTTGTAGTTG ATAAAATAATCAAATCGTCATAATGAACCGAGATAT AGCATTTCAAAGTGAAATAGTGGGCTGCAATAGAG GAAATAAGGTAATTTTCCCTCACCCCCTTGACTATA CAACACTCTTGAGAGTATCCATGGACAACAATCAT CGTACCTTAATTAACCTACCTTAAGCCTCCTCCCA ACCTCTCCATCTCTTCCGTTCAATATGATACCTTCA TTTCCCGCATCTCGGGGGCTTAATCCTCTTTCCTT CTCTTCCTCAAGCGGCTAATGAACATGCACTCATT TTCAGGCACCACATTTCCCGCTTGCTTTTCTTGCC GCCAATCCAGAAGCGTACAAACTGATGCAGCAGA CGACGTGTGCATCTCCAGATGCCGAGTGTTCCAG GTTTGTGAATGATTTATATGGTGAATCAAAAAAAAA GTGGAGTAGTTCTCTTACTCTTATCAATAATTGATT TATTCTATTCACTCTTTAGTACTAGTGAGAAGCTAA TATATTGTATAGAAAACACAAAAAAAAATCAATTTA TTCCAGTGGACATGCCAGTGAATCTTCACCAACTA CAACTGAACCAGTCGACCTAACAGCTACACCAAAA CCTCCTTCGACGTCTGAAATGGAAACTACATCAAA GTCCGACGATGGAGAGGATCGTGACAGCATCGGA GACTCTGGGAATGATGATGATGATGACTCAGAAGC TGGAGTTCTAGATGAGTCGTCCACAACAACGTCAA CGAAAAAGCGTCCGACATCTCACACAATTTCCGAC ATACTCGCTGCTCCACAACTCGGTGCTCAGGCTTT GAATTCGACGTTCCTTGGCATGCTTCAGCGCTCGC TTAATTATAATCCAGCAGTTCCATCGCCTCACTCAT TTC
egl-43L (N-terminus)	gatgctcatcctgaaaactt	TATTTTCCGTCCAGCAATTTACTTCCAAAAATTCA AACTAAGTCAATAGTTGTTATAGTTTTTAAGTTGG TCTTTGATTATTGAGCAGTTCGGTAAACTCGCAG CCGACCTCGATGGAGTCTCGCGATAGCCTACTC CTGGAAAAAACGTTTGTCTTCTGCTTTCACCTCAT GATATCAGGAAACTTATTACAGACATTCAGCCGA CAAATAAACGGCTTGGCTTCTACTAGAAATGCTC AATAGATTCTAATTTAGTAGGTGTAGATATTTTCA CTTTTGTTTATTTTTCTAAGTATCGAAGTACATATG TTAGAAAGTAAATAAAAATTGCTATTCTACTTTAA GAATTTTCTATATTAAAATAGTCTTTAGTAACGTG GGGTTTTCGAAACTTGCAACTTTTCAAGTGAAGAT GCTCCTCACCTGAAGCATCCTGTCACTCTACCGA TTGGCTGATGGGCGTGTCGTCTTCCATCTCTTCC ACCCGCCCACTTTTTGAGACAGGAGAGGCTCTC GCTCCTCTCGCATCCACAAATGGAAGGCGCCTCT TTCCATCTTCCTTTCTTTTTTTTCTGGTTAGTTGAA GTATCCTTAAAGTATCTTGACGTTTTTACTATATAT GACTTCTGGAGAGACATTCGAGTTTTTGGATCAA ATATAGAATGTCAAATTTTGAAGAGCAATCTTCTC ATATGTCAATTTTTCAATAAAATTGTATCCTACATT GTGGTGGTGTAGAACCCTCAAAAAATAATCTCTA AATTAAGAATTTCTTGATTTTAAAACTGACTAGCA AATTTGTCATGAAAAATCTCAAACGAATTTCCTAC AGTTCATCTACCAAATGAATTGGGCTTGTAAACTT TTTCACCATCTACTAAAAAATTCAATAAAATAATAA TCTCTTCCCAAACTACACCTCCCTCCAATATCTCT CAGCTTACTCCTAACTCCTATCCCAAATTCGTACA TCTACCGTACCATTCCTCCTCCCTGTTCGTTCTCA ATGACAAAGCCAGCCTTGAACAGCCATATCCAAC TTTTTCGTTGCATTGTTCTCGTTCACAAGATGTAT TACTCATCTTTCGCCCCAAAACTGTTCTTGTAATT TGTACAGTTCTTGTTTCTTCCCACGTACAGTTTCC TAAGTTTTCAGG	ATGAGCATCGACACAGACTTCCTCACGAGTGTTGA GGTAAAGGAGGATGAGCTACATGGAAATGTGCTC ATTGCAGTAACTCAAATTGCACTCGGAAGGACCAT CGGTGTGATTGATAAGGTGAGCTTTTGGTGTACAA TTTTTACGCCGTAGACATTGTCTTAGAGGTGTCCG CTAGAAAAAGAAGTATAAGCTTATTCCCGGGCGTC TAAAAAACTCCACCGGAAAAAATACAGGTCGCTTG AACTGAAATATCTTATAGCTTGAGTAACCTATGAAA TAAGCTTTCAGATGTTACACTCATATTTTGTTAGTT AGTAGTTATATGATAACAGTAATTTTAGGTTGTAAT TGATAAAATAATGACTTTTTTAAATTAACAAAACTTT TTTTAAAATATTTTTACAAGCATTTTAAATTGATACC TTGGTGCCTAATCTACCTAATCTACAGTACCTTCG CCAACATTTTCAAATCCTTTCCTAATGATTCAACGT TCGAATTACAAATTCTTCCCAGAACCCAAAACCGC AATTATCGGGACCCTGAAATGTTTGGCGCCATGTG TTCCTCCCTGCTTCTTCTCCTCAAAAATTCCTTACA CCTGTCTTTCCACCTTTCCCGCTCCCCCCGTCCAT TACCACTTTGTTAACCTTGGGGGCACACTAGTAAC CATTACATTAGGATTTA

fos-1A (N-terminus)	ccactctcttatatagcaga	CTTAGACATCCATCCAAATATTTAAATGTTGCTGT TGCTTTTGGGTCAACAAACGACACATACCTGTTA GTGTCATCCTTCGTTCCGCGTGCACGCATCGCAC TGAATCATCGGTATTCATCACCTCTTCTCTGCAAT CAACGAGCCAAATGCCAATTGGGTTATTTGAGTT AGAAACTCGGGAAGCTTCACAGAAGAAATAATTA GCTGAATTGGCAAAGAGAGCACCTGCTCCCCGG AATGTCATACTTTTGTAGAATAAAAGAAGGGAAGA CGACGACGTCTCCGGTTCTTCTATCCCAAACAAT ACCATTTTTTGTTTCCCATCTCGTCTTCGATGTTG CTGACTCACCATCAATATCTAAACAGAAAGCACC CAATGGTTCGCCTTTTTTGTCTCCTTTCTCGACAG TTTCTGTTTTTTTTTGTATGTTACATAAATACCGTA CACCCACCATCTAGTCAATTGTCACATATTCGAAA TCAAAAGTTATCAAAAACTCTCGTGCACTTTAATA CACAGTTCCGTCGGCCACCCCGTCACCAGCCGG CGTTTTCTTGGTGATATCATTGGCGGTGGCTCTT TGAAAATTCAAATTTGGTGTCGTCCTCCCGAAGG TGTGGGCGGAGCTTGCGCACCGTTCGCGGTGGC CGTTGCTCTCGACAGTTTTCTCTTTCCCTCGCTC CTTTCTTCTCTCAACCAAACACCTGCCCACACAC GCAACTTACTTTTGTCATCGCTGGTCCCCTGTCC AAAGATACAATCAACCCGTGTTGTGCTAATCATCA CCTAGAAGAGTCATCTTCGTGAATCAGAATCCCT TTTCTTCCCCCTACTTTTTCCACTTCTATTCCCGG TTACTCACCTTCTGTGTTTGGCCCCGATCGTGTG TCAGCACGTCTGCTATATAAGAGAGTGCA	ATGTTCGAACAACCATCGTCGACGACTAACACCAC CACGAGCTCTGGTTCTGGCTCCGATTCCAATCACT ACTTCGAATTGGGTCCCAGGAACCCGATCAACCAA GCGCACCCGACATCAGTCATTGTTCCACCGCGAC AACATCACCATCAGATCCACCAACAACAAACCGAC AACTCACCTCTAACTCCGTGTACACCATATTATCCA TCAAATGCATATGGACTCCCTTTATTCTTTGGAACT GATTTCCTGCAGGTATGATACATCACAAATATCTTC CTTAATTCAGTGTTTACTTCAAAGTCCACTATTCCC TTGCTAATAATCACGAGTTTTGATAGAGCTTTTAAA TCATTACTTTCACTCATTTTTCACTCAACCTCGAGC CTTACATTTGTCAGTTGATCTCTTCTTTCCCATATA AAAATGAGATTATAGTAGCTTACTTTCATTTAGTTT AATATTAATTCTGAAAGTATCAAACCAAAAAGTAAA GCGTTCACTAATTCTTTTGTGCAAAAGTCATGCAG AAAAAAGTTACCTAGCTCTTGAATCTTTTCCCTCAA AAATGTTCTTACCAGCCATCTCCCCCGGATTTTAG TTCCGGAAAAATAAAACTATTTGGTTATGGATTAAA TGTATATGGATAGGTGGTGCACGAGGAATCTTAAA AGAAGATGCCGACGTGTTTACACACTTCTACAGTA ATCTATCTATCTTTCACCTTTCCCCCAATTGTTACT TTTGTGATCTTCTTTACCTCTCATGCACTCGCTAAT CCGTTTTGGATTGTTTCCTGTTTGCACCTGTTGAAA AAAGATAAGTAATACTTATATGTTAACTTTTTTCGG TGCCAGTGAAAATATTACAGGCACGCAAATTTTTTA AATATTCAAAAAATATCTGTCACTTCTGCTTTGAGC TTG
hlh-2 (N-terminus)	agttttcagaacctcaatgg	GACTGGTGAATGAATGGTGGGAGAAGAGATGGA GGACCCCGGGATAATAGAGGATTGTGTGCTGCA GGAGGTAGAGAGAGATGGTTGTGGGCGTGACCT CTCCCGATCATCGTCTCTGCGTCTCTTGGATGTA GACGGTCCCCGGGAGAAAGAATGTCTGCGTCTA TGTACACCAATATACTGTTTATGTCCCTTGAATGG GCTTTTATACGCGTCCCTCCACTACCACCACCCT CGAAGAACCATTCCTAGCCACCCGCATAGCCGCT AAGAAGGGGGGAGTGCACTCTTTTCGTCTTTTTT TGTGTCTAAATCTGTTCCGTTTACTAGCTTTTCAA GTTCATGATCTTACTGTAATAAAACATAGCACATA TTTTGAATGAAATACATAATGTATCCCATCTTCTG ATTTTGAAAATTAAAATTTCTCTCCTCCCAATTTTC AATTTTGGATCTTTTACCAAATAATTTTGATCTGCA TTACTTTTTCTCACTCCTACAATGTTTACGAATCC TTACCAATTTTGAATTTAAACAAGAACGCAAATGT ATTGTAGGGCAGTTTTTTTTTCAATTATTGAGTTTA TCAAAAAATGTATATTTGCATCCGAAATGTTACTA GCTCACGTTTAAAGCTTTCATATATATCTTATCCT ACGTCTGAATTTAAACTAATTATTTAGATGGGCCT GAAACCCTTTGATCCATCACCCCTTTACTGTTATT TTATTGCTCTTTCGGGATGTCATCCATCCGATAAT CATCTACAATGACATCTACATTTACAACTATTTCTT GATACCATCTCAACATCATTACCTCCCTACAAATT GTTCTCCTTCAAGTAACTTGCTCCTAATAATTTAT ACCGGAACTTAGTAGATCTATTGTGACGTCACAA TTATTATTCTTTATTGATCTACCTTGCCTCTTTTGA TCTCGTTTGCCTATTTAACCAAACGAGGAGAATC GATTATTTTCTTCTTTTTCTTATTCTCAATATTTCTT CAAATGGGGTTGTCTTGACGAAAATCTAATCAGA ATATATTTACTAACCTAATTTTTTCACCTGCTGCTC CAGCCCAATTCCCTACTTATTCCCTTTCCTCTCCC CGCTTCTCCGCTGACTTTATTTCTTTGACATTACT ACTATAATCGTCTTTCATATCATTTCGCAGAAATA AAGTTTTCAGAACCTCA	ATGGCGGATCCAAATAGCCAACTTACGTCAGCCAC AACTGTTGCAACTGCCGCCATTGCTCAACCACAGG TTATGCTTCCAAATGCATATGATTATCCTTATAATA TTGATCCGACAACGATTCAGATGCCTGATTATTGG AGTGGTTAGTCTTTTTTTCATTTGAAATCTATTATAA TTTCAATTATATCATTTGGTAAACCAAACCAAACAT GTTTTCGTGAATTTGTTAAAAGTCGCTTGTAATCAG TTAGAAATATTGGATAAATTGCAGAAAAAGGATATA AGTTTGGTATTACTTATCTCGAATTGTTGAATTGTT GATTTTATAAGCTCGCAAATTTTTAAAATTTACTTTA AGTTGAAACAAAATGTATAACTCTTTTAATGTTCTA AAATTTTGTAAAAATCTGGTTTGCTCTAGTAAGTAG TTTATTAACCAAAATGTTTATATCTCATTTCTCAAGT GCAAGTCATCTAAATAAACATTTTCAGGATACCATC TCAACCCGTATCCTCCGATGCAAACAACGGATATT GATTATTCATCAGCCTTCCTTCCAACACATCCACC AACTGAAACCCCTGCTTCCGTAGCTGCTCCAACTT CTGCAACATCTGATATTAAGCCAATTCATGCAACAT CATCCACTTCAACGACGGCTCCATCTACTGCTCCA GCTCCAACTTCAACTACTGATGTGCTTGAGTTAAA GCCAACAACAGCTCCAGCCACGAATTCTGCAGAA ACATCAGCGATTGTTGCTCCACAGCCTCTTACTAA TCTTACCGCACCAATTGACGCAATGTCATCAATGT ATACATGGCCACAAACATATCCAGGTTACCTTCCA CCTTCAGAAGATAACAAAGCAAGTGAAGCTGTTAA TCCATACATCTCAATCCCTCCAACATATACATTTGG TGCTGATCCATCAGTTGCCGACTTCTCATCGTATC AGCAGCAACTTGCTGGACAGCCGGTACGTTTCTAT TCTTCTTGGTTTTATTCGTGTTTTACTGTTTTACCA CAAGTTAATCTCGACGAATGATTGCTTGGCCCTCC TCAGCCGCCAAGCATTCACGTATGCATAATCCGCT TCCTTTTGATGTGAGCCGCCGCCTTCTGAAGATTG AGATGCATGCAAAAGGCGGCATCTTCTTGAGAAGA ACACCCTGTGCGCACTAAACGACCTCC
nhr-67 (C-terminus)	ccacgtcattcgattcgatcaat	N/A (made by SunyBiotech)	N/A (made by SunyBiotech)
	agagagtgttaatgttgaagagg		

Table S7: RNAi vectors

RNA Target	Synthetic gene block
egl-43L(RNAi)	TCACTATAGGGAGACCGGCAATGAGCATCGACACAGACTTCCTCACGAGTGTTGAGGTAAAGGAGGATGAGCTACATGGAA ATGTGCTCATTGCAGTAACTCAAATTGCACTCGGAAGGACCATCGGTGTGATTGATAAGGCTACACCGAATGATTCGAATGC TCTTCTCATCTTGAACCTGATTAAGGAAGCTGATGACGGAGAAGATGCCAATATTTGTATGAGGCAGGAGGATAGAAAGACT TTTCTACAAACCAGTAAGATTATCAATATTGGAGAGCGTCTTCTTCTACAAAGACTGTCCGAAGAGGAGTGTGATGAGGAGG ATCAGGATGATCTTGAGAATTTAATTTTGTTAAAAGATGAAGATCGGCCGGACAGTACTCAAAGCTGCACAAAGAGCAGCAG TGAAGACAGCAATCTAAACGGTTTCGAGGAGTATATTCGAGAACACGGCGAACTTGTACCTGGTCAAACGCCTCCCGACGG ATCACACAAGTGTGGAGTTTGTCCAAAGAGTTTTTCAAGTGCAAGCGGTCTCAAACAACACTCTCATATTCATTGCTCCTTAA AGCCGTTTCGGTGTCATTTGTGTCCAAAGTCCTACACACAATTCTCAAATCTGTGCAGGCACCGGAGAGTTCATTCAGACGG TTGGACGTGCCCAACGTGTCAAAGTCAGGGGGGGGGCCCGGTACCCAAT
egl-43(RNAi)	TCACTATAGGGAGACCGGCAATGCCATCACAAGCGGCACTAACGAAGCATCGACCAGTTTGCGAGATGACTGCACTCTACA AACCATTGATGGCGCAACTTGCCGGATTGAGCGGAGCAGGTGGATTAGGTTCCGTGCCATATTGGCCACATATACTTCAAAT GGCAACACAGGCACCACATTTCCCGCTTGCTTTTCTTGCCGCCAATCCAGAAGCGTACAAACTGATGCAGCAGACGACGTG TGCATCTCCAGATGCCGAGTGTTCCAGTGGACATGCCAGTGAATCTTCACCAACTACAACTGAACCAGTCGACCTAACAGCT ACACCAAAACCTCCTTCGACGTCTGAAATGGAAACTACATCAAAGTCCGACGATGGAGAGGATCGTGACAGCATCGGAGAC TCTGGGAATGATGATGATGATGACTCAGAAGCTGGAGTTCTAGATGAGTCGTCCACAACAACGTCAACGAAAAAGCGTCCG ACATCTCACACAATTTCCGACATACTCGCTGCTCCACAACTCGGTGCTCAGGCTTTGAATTCGACGTTCCTTGGCATGCTTC AGCGCTCGCTTAATTATAATCCAGCAGTTCCATCGCCTCACTCATTTCTAAGAGCAATGAGCGGAGCAAAAGCATCATCATC ACCAAGCTCGAGCAGTGGAAGTGGAAAGGATAGGTACACGTGCAAGTTCTGTCAGAAAGTGTTCCCAAGATCAGCGAATTT GACAAGACATTTAAGGACACATACAGGAGAGCAGCCTTATAAGTGTCAATATTGCGAGCGAAGCTTCTCAATCTCCTCCAAT TTGCAACGCCACGTTAGAAACATTCATAATAAGCCGAACACCTCGCTGACACCCCACAATCATCATCGTCAACGAAGTCTGC ACAATTCAACCTCAACCTCCACTACTACTACTACCGTCCATCATCCTCTTCTTCATCTTCCAGGAACGTCCGTTCCGGTGCCA AAAGTTACCGGGCCCCCCCTCGAGG
fos-1(RNAi)	CTCACTATAGGGAGACCGGCAGATCTATGGTACAGTATAGCACGGTGAAGAAATCGTCGGCTGGGAGAAAACCTAAAGAAG AGGATAATATGGAGGATGACGATGATGATAAGAGGCTGAAACGTCGTCAAAGGAATAAAGAAGCTGCTGCAAGATGTCGGC AAAGGAGAATTGATTTGATGAAGGAATTGCAAGATCAAGTAAATGACTTCAAAAATAGCAACGACAAAAAAATGGCGGAATG CAACAACATCCGAAATAAGCTCAACAGTCTCAAAAACTATTTGGAAACGCATGATTGTAAACTGAGTCGCGAAGAACGAACA CATGAGATAAATCGATTGATAATCCCACCATCAACAGTTCCACCATCACAACCATATCTTCAACATTCGTTGAGAGTTCATCC ACCACGTGCTGACTCTGTACCATATTCTATTCGATCAGGACATTCATCTTCATCGTCTGAACAACACTCACCAGTTGAGGACT ATAAGCCTTCAATTGATCAATTACTTCTTCCTCCAATCTCATGTATTCAAAATATCAAAGATCGAAATATCAATTCTATGCCACC ACCAGCTTTACCGGCAAGCACGAGTGCTGCTGGAATTCATGTTATCACTTCTATCCCGGTTTCGCATGCCAACTCATTACAC GGTCGTTCGGAAAACGTTTTCGCAGAACCGGAACGCAAAATTCCAAAAATCGAGTTGGACCAAACACTGACATCATTGACCA TGCCAGACGACGTTGAACGTCCGTCAGCTCTTCCGACGCTTTCCAGAATCGTTGAAAATCAGCCGATCACTACTCCCAGCA GGCCTTTCCGTCTCGGGGGGGAATATCAAAATCAAACACCGCAGAGTACAGGGAATGGACTATTCGGAGGCCCACCAGGC CCATTCGACTTGCTTTCCTCCAACACTGGTCTGACACCTTCTGGTCAGCCAACAATGAACTTCGTTTCAACTCCAACCCCGAT TCAACCACATCCGGATGCTGATCTCCGACCACTCTAGGTCGACCTCGAGGGGGGGCCCG
hlh-2(RNAi)	TCACTATAGGGAGACCGGCAATGGCGGATCCAAATAGCCAACTTACGTCAGCCACAACTGTTGCAACTGCCGCCATTGCTC AACCACAGGTTATGCTTCCAAATGCATATGATTATCCTTATAATATTGATCCGACAACGATTCAGATGCCTGATTATTGGAGT GGATACCATCTCAACCCGTATCCTCCGATGCAAACAACGGATATTGATTATTCATCAGCCTTCCTTCCAACACATCCACCAAC TGAAACCCCTGCTTCCGTAGCTGCTCCAACTTCTGCAACATCTGATATTAAGCCAATTCATGCAACATCATCCACTTCAACGA CGGCTCCATCTACTGCTCCAGCTCCAACTTCAACTACTGATGTGCTTGAGTTAAAGCCAACAACAGCTCCAGCCACGAATTC TGCAGAAACATCAGCGATTGTTGCTCCACAGCCTCTTACTAATCTTACCGCACCAATTGACGCAATGTCATCAATGTATACAT GGCCACAAACATATCCAGGTTACCTTCCACCTTCAGAAGATAACAAAGCAAGTGAAGCTGTTAATCCATACATCTCAATCCCT CCAACATATACATTTGGTGCTGATCCATCAGTTGCCGACTTCTCATCGTATCAGCAGCAACTTGCTGGACAGCCGAATGGTC TTGGTGGAGATACCAACTTGGTTGACTACAATCATCAATTCCCACCAGCCGGTATGAGCCCACACTTTGATCCAAATGGATA TCCAGGAATGACCGGAATGCCACCAGGATCAAGTGCATCATCTGTTCGAAATGATAAGTCTGCATCAAGAGCAACGAGCCG TCGTCGGGTACAAGGCCCTCCATCTTCTGGAATTCCAACTCGCCATTCATCGTCTTCAAGGCTTTCTGATAATGAATCAATGA GTGATGACAAAGATACGGATAGGAGATCACAGAATAATGCTCGAGAAAGAGTACGAGTTCGTGACATCAGGGGGGGCCCG GTACCCAAT
nhr-67(RNAi)	TCACTATAGGGAGACCGGCAATGATGACTGCGGTTTCACAGATGTCGGTTCCAAGCAGTCGAATTCTATTGGATGTTGATTG TAGAGTCTGTGAAGATCATTCGTCGGGGAAGCATTACAGTATTTTTTCCTGCGACGGGTGTGCTGGATTCTTTAAACGTTCAA TCCGTCGTCATCGTCAATACGTGTGCAAAAACAAAGGCAGTCCATCCGAAGGACAATGCAAAGTGGACAAAACACACCGCA ACCAGTGCAGAGCTTGCCGACTAAGAAAGTGTCTGGAAATTGGGATGAACAAAGATGCTGTCCAACATGAGAGAGGGCCTC GTAACTCAAGTTTAAGACGACAACAGATGATGTTCGATCATGGATCCTCTCCTAATTCGCCGGAAATGGGATCAGAAAGTGA TGCAATAATTCTTCCGACATCATCAATGAATCGTGACACAGTGGCCGGTACTGCTGCTCGAATCTTTTTTGCACTTGTTGGAT TTTGTCAGAATCCTTTGAATGGAGTACCTAAAGAACGGCAAATGACAATGTTTCAACAAAATTGGGCAGCACTTCTTGTTCTC CATGCAACTGAAACACGTGCCATAACTTCTAAGCAAATAAGGACTGAGACGATATCCGGTAGCTCAGAGCAAAGAAATGCG GTTGCTAACGCGTTTGAAATAATTGAACGTTTACAATTGGATAATAGAGAATACATGATGTTGAAACATTTCACAATGTGGAG AGATACACCAAGTGCAATTCAAATTGTCTTTCAGTTAGCATCTATTCAGAATTTCACACATAGAACCGAACCGACGAGATATA TCCAATGTATAAATGCAATTGCCGCTATTCCAACAACTTCAATAATTGATGTTCTATTCCGCCCTTCAATTGGATCAGCTTCAA TGCCAAGACTTATTCAAGACATGTTCAAGCCACCACAACAACCCACTCCTACGTCACTGTTTCCAATGGGGGGGGGCCCGG TACCCAAT